NUMERICAL SIMULATION AND PREDICTION OF LOADS IN MARINE CURRENT TURBINE FULL-SCALE ROTOR BLADES

by

Junior Senat

A Thesis Submitted to the Faculty of

The College of Engineering and Computer Science

in Partial Fulfillment of the Requirements for the Degree of

Master of Science

Florida Atlantic University

Boca Raton, Florida

May 2011

NUMERICAL SIMULATION AND PREDICTION OF LOADS IN MARINE CURRENT TURBINE FULL-SCALE ROTOR BLADES

by

Junior Senat

This thesis was prepared under the direction of the candidate's thesis advisor, Dr. Madasamy Arockiasamy, Department of Civil, Environmental and Geomatics Engineering, and has been approved by the members of his supervisory committee. It was submitted to the faculty of the College of Engineering and Computer Science and was accepted in partial fulfillment of the requirements for the degree of Master of Science.

SUPERVISORY COMMITTEE:

M. Arockiasamy, Ph.D., P.E.
Thesis Advisor

Howard R. Hanson, Ph.D.

Chadi El Ghenai, Ph.D.

Yan Yong, Ph.D.

Panagiotis D. Scarlatos, Ph.D.
Chair, Department of Civil, Environmental and Geomatics Engineering

Karl K. Stevens, Ph.D., P.E.
Dean, College of Engineering and Computer Science

Barry T. Rosson, Ph.D.
Dean, Graduate College

April 15, 2011
Date

ACKNOWLEDGEMENTS

The work presented herein has been supported financially by the Southeast National Marine Renewable Energy Center (SNMREC) and the author gratefully acknowledges the support. The author would like to thank Susan Skemp, Executive Director, and Dr. H.P. Hanson, Scientific Director for the constant encouragement.

The author wishes to express his sincere thanks to his thesis advisor Dr. M. Arockiasamy, Professor and Director, Center for Infrastructure and Constructed Facilities, Department of Civil, Environmental, and Geomatics Engineering, for his excellent guidance, suggestions, and constant review in all stages throughout the course of this work. Grateful acknowledgements are due to Dr. Yan Yong and Dr. Chaouki Ghenai for their interest, encouragement, and manuscript review. The author expresses sincere appreciation to Professor N.Baltrop at the Department of Naval Architecture and Marine Engineering, University of Strathclyde, Glasgow, UK, for providing the computational tool used in the present study.

Finally, I am most grateful for the support, affection, and encouragement from my parents, family and friends throughout the course of the research.

ABSTRACT

Author:	Junior Senat
Title:	Numerical Simulation and Prediction of Loads in Marine Current Turbine Full-Scale Rotor Blades
Institution:	Florida Atlantic University
Thesis Advisor:	Dr. M. Arockiasamy, P.E.
Degree:	Master of Science
Year:	2011

Marine current turbines are submerged structures and subjected to loading conditions from both the currents and wave effects. The associated phenomena posed significant challenge to the analyses of the loading response of the rotor blades and practical limitations in terms of device location and operational envelopes. The effect of waves on marine current turbines can contribute to the change of flow field and pressure field around the rotor and hence changes the fluid forces on the rotor. However, the effect of the waves on the rotor depends on the magnitude and direction of flow velocity that is induced by the waves. An analysis is presented for predicting the torque, thrust, and bending moments resulting from the wave-current interactions at the root of rotor blades in a horizontal axis marine current turbine using the blade element-momentum (BEM) theory combined with linear wave theory. Parametric studies are carried out to better

understand the influence of important parameters, which include wave height, wave frequency, and tip-speed ratio on the performance of the rotor. The periodic loading on the blade due to the steady spatial variation of current speeds over the rotor swept area is determined by a limited number of parameters, including Reynolds number, lift and drag coefficients, thrust and torque coefficients, and power coefficient. The results established that the BEM theory combined with linear wave theory can be used to analyze the wave-current interactions in full-scale marine current turbine. The power and thrust coefficients can be analyzed effectively using the numerical BEM theory in conjunction with corrections to the tip loss coefficient and 3D effects. It has been found both thrust and torque increase as the current speed increases, and in longer waves the torque is relatively sensitive to the variation of wave height. Both in-plane and out-of-plane bending moments fluctuate significantly and can be predicted by linear wave theory with blade element-momentum theory.

NUMERICAL SIMULATION AND PREDICTION OF LOADS IN MARINE CURRENT TURBINE FULL-SCALE ROTOR BLADES

LIST OF FIGURES

LIST OF TABLES

NOMENCLATURE

a	axial flow induction factor
a'	tangential flow induction factor
A	foil area
c	chord length; celerity or phase velocity
c_l	lift coefficient
c_d	drag coefficient
c_m	moment coefficient
C_p	power coefficient
C_T	thrust coefficient
d	water depth
ds	rotor axis depth
D	diameter of the rotor
f_e	encounter frequency
H	wave height
k_w	wave number
L_w	wave length
M_{ipb}	in-plane bending moment
M_{opb}	out-of-plane bending moment
n	rotational speed (rev/s)
P	power
Q_{jt}	torque
R	radius of rotor
Re	Reynolds number
R_W	wake radius
T_{jt}	thrust
T_w	wave period
u	wave particle velocity in horizontal direction
v	wave particle velocity in vertical direction
U	free stream velocity
U_c	current speed
zr	instantaneous vertical position of centroid of blade section with respect to rotor axis
α	angle of attack
β	inclination of local chord to rotor plan (i.e., blade twist plus pitch angle, if any)
θ	incident angle of current
θ_w	incident angle of wave
ν	kinematic viscosity of water at 20 ^oC
Ω	rotational speed of the rotor
λ	tip speed ratio
ϕ	angle between incident flow and the chord
ϕ_w	phase angle of wave
ρ	water density
μ	non-dimensional radial position

Chapter 1

INTRODUCTION

1.1 Background

Different energy resources in nature ranging from ancient water wheels and wind mills to modern hydropower plant and wind turbine have been utilized by human to generate power. Tides were first used in tidal mills to ground grain throughout the Middle Ages. For instance, the first commercial scale tidal generating barrage rated at 250 MW was built in La Rance, France in 1960. This plant continues to operate until to-day (Charlier, 2007). Nowadays, the world is heavily dependent on fossil fuels which account for 74% of the global energy consumption in the form of coal, petroleum and natural gas. These resources are on the verge of exhaustion and their excessive use has given rise to severe environmental pollution and climate change. Hence, global interests have shifted to the development of new and renewable energy as an integral part of the future energy strategies (Wang et al., 2008). Therefore, increased awareness among the energy community has become evident in renewable energy resources such as wind energy, solar energy, and small scale hydropower schemes. These resources have great potential to meet the world's energy demand for the 21st century and beyond with a clean, safe and

economical environment. However, the intermittency and weather dependency of most of these resources still poses a challenge and calls for extensive and diligent research developments.

1.2 Marine Current Resource

Marine (or ocean) currents have gained tremendous worldwide attention and consideration for clean power generation. They represent large movement of seawater driven by wind and solar heating of the waters near the equator, although some ocean currents result instead from variations in water density and salinity. These currents are relatively constant and flow in one direction only, in contrast to the tidal currents closer to the shore where the varying gravitational pulls of the sun and moon result in diurnal high tides. Some examples of ocean currents are the Gulf Stream, Florida Straits Current, and California Current. The Florida Straits Current starts only 8 km offshore in the southern part of Florida, close to Miami, and sustains relatively large speeds over significant distances in relatively unchanging patterns. Marine currents tend to be concentrated at the surface, although significant current continues at depths below ships' drafts.

A few completed resource assessment studies indicate that ocean currents have the potential to supply a significant fraction of future electricity needs. The total worldwide power in ocean currents has been estimated to be about 5,000 GW, with power densities of up to 15 kW/m^2. The relative constant extractable energy density near the surface of the Florida Straits Current is about 1 kW/m^2 of flow area. It has been

estimated that capturing just 1/1000th of the available energy from the Gulf Stream, which has 21,000 times more energy than Niagara Falls in a flow water that is 50 times the total flow of all the world's freshwater rivers, would supply Florida with 35% of its electricity needs (MMS, 2006; IEA, 2003). The Florida State Legislature sponsored a project under "2006 *Florida Energy Act*" and found that the Florida Current has a potential generating capacity of up to 10 GW (Driscoll et al., 2006).

The gross kinetic energy in marine currents is extremely large and predictable. Although, marine current speeds are generally lower than wind speeds, they carry a large amount of energy because of the density of water. Water is more than 800 times denser than air, so for the same surface area, water moving 12 miles per hour exerts about the same amount of force as a constant 110 mph wind. This is a unique renewable resource that is relatively potent and independent of random weather conditions. The Florida Current off of the southern and eastern shores of Florida represents 20% of the Gulf Stream and North Atlantic Gyre, and has a significant hydrokinetic energy available in its moving water. For successful exploitation of this resource, an understanding of the hydrodynamics performance of the energy converter systems is of primary importance to extract this energy.

So far only a limited number of marine current prototypes and demonstration units have been tested in the US and Europe. To date, there are no commercial grid-connected turbines currently operating. Some of these technologies have been developed for use with tidal currents in near-shore environments. For example, one of the main tidal energy turbines installations is the twin rotor horizontal axis tidal turbine (HATT) system

in Northern Ireland has a rated power to a maximum of 1.2MW and now connected to the electrical supply infrastructure.

1.3 Renewable Energy Extraction Systems

The two most sustainable forms of renewable energy conversion systems use kinetic energy conversion (KEC) and ocean thermal energy conversion (OTEC) systems. OTEC uses the thermal gradient produced as a result of the heat absorbed by the sun at/near the surface and the much cooler water far beneath the surface to produce energy. KEC is associated with waves, currents and tides, producing energy using a turbine or wave buoy. Kinetic energy from marine currents can be harnessed using relatively conventional systems, following the principles similar to those for extracting energy from the wind energy (Lemanski et al., 2008). Two of the most common kinetic energy devices that have been developed use horizontal-axis and vertical-axis rotor turbines. Vertical-axis rotors are subject to cyclic loading even in uniform flow, and in tidal streams, these will result in fatigue loads, which will make the structural design more complex. However, horizontal-axis wind turbines have achieved a dominant position in the wind energy market, and design for tidal streams can take advantage of buoyancy to balance the weight. Horizontal-axis devices have relatively low level of turbulence which reduces stochastic structural loads; however, deterministic cyclic loading may be comparatively large.

Current applications of land-based Horizontal Axis Wind Turbines (HAWT) are very well established and installed all around the world to generate clean energy many in

large arrays, as shown in Figure 1.1.

Figure 1.1: HAWT arrays in Palm Springs, California.

Most of the modern commercially available and utility scale wind turbines from established turbine manufacturers utilize the 'Danish concept' turbine configuration. This configuration uses a horizontal axis, three-bladed rotor, an upwind orientation, and an active yaw system to keep the rotor oriented into the wind. These turbines have rotor diameters between 30 and over 100 m that operate at much lower rotational speeds. Also, noise emissions vary by the seventh power of the blade speed, so a design with a larger rotor diameter operating at a lower *rpm* will essentially produce less noise than the power producing equivalent smaller rotor diameter HAWT operating at higher *rpm*. Over the last few years, turbines with rated capacity of 1.5MW to 3.6 MW have been installed onshore and offshore in the world. In terms of installed power, the main project included the following: in the US, the Roscoe Wind Farm project (780 MW) and the Horse Hollow Wind Energy Center (700 MW); in the UK, the Thanet Offshore Wind project (300

MW), the Lynn and Inner Dowsing (194 MW), and the Kentish Flats project (90 MW); in the Netherlands, the Q7 project (120 MW); and in Denmark, the Horns Rev II project (160 MW), the Rodsand II project (207 MW) and the Nysted offshore Windfarm (165 MW) [ISSC V.4, 2009,].

However, land-based renewable energy technologies are already facing constraints owing to conflicts over land use, thus the seas offer a large open spaces where future new energy technologies could be deployed on a large scale with a less impact on either the environment or other human activities. Over the last few years, a number of offshore wind farms have been put in operation in European countries such as Denmark, United Kingdom (UK) and the Netherlands. They are all situated in shallow waters, having water depth of less than 25 meters and are relatively close to shore. For these developments, it proved economical to either use simple concrete gravity structures or steel monopoles as substructures. Fig. 1.2 shows some of the typical substructure and foundation designs for offshore wind turbines. While the U.S. has a long history of onshore wind power development, offshore wind power resources remain largely untapped. Only a few offshore wind farms have been proposed for U.S. waters, but none have yet been constructed. Most recently, the investigation of using floating wind turbines structure in very deep waters (Fig. 1.3) is carried out in many countries due to the corresponding decrease in availability of shallow water sites. Significant efforts have been made to implement this modified wind turbine structure, especially in Norway, the United States of America and Japan. Above all, the functionality and survivability of a system operating in an underwater environment demands simplicity and robustness.

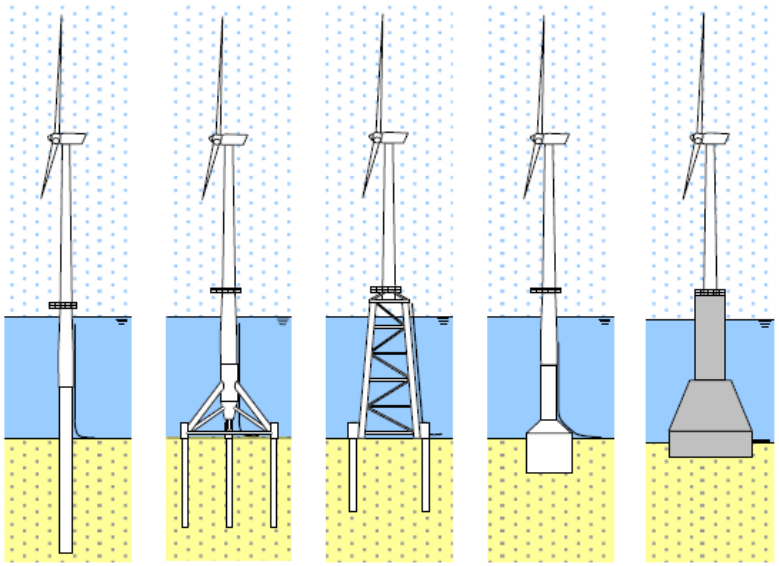

Figure 1.2**:** Typical fixed support structures (W.E. de Vries *et al.*, 2007): monopile, tripod, jacket, suction, gravity base)

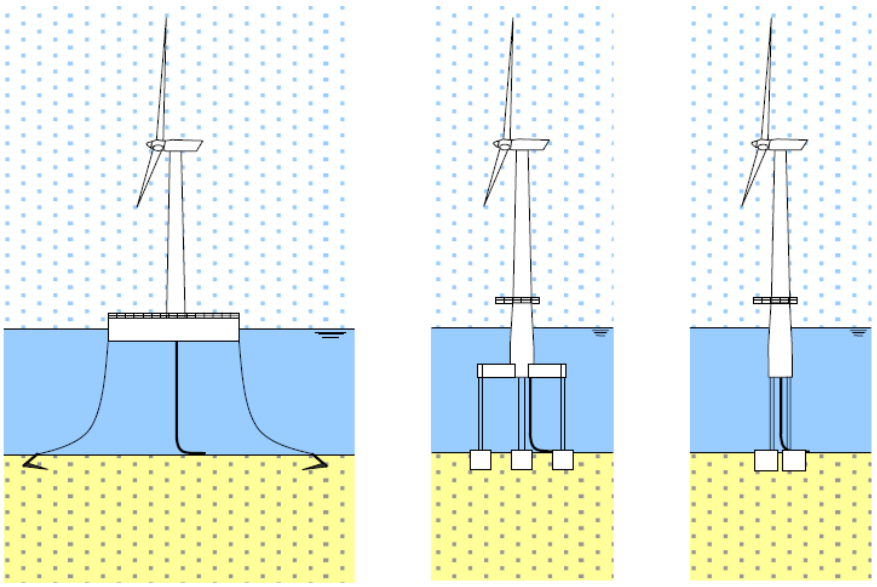

Figure 1.3**:** Typical floating structures (W.E. de Vries *et al.*, 2007)

1.4 Scope of the Thesis

The objective of the present study is to carry out numerical simulation of the dynamic characteristics of a full-scale rotor blade of a horizontal-axis marine current turbine and predict the torque, thrust, and bending moments. The measured current velocities taken near the core of the Florida Current offshore Fort- Lauderdale, Florida are used in the evaluation of the loads on the rotor blades. The periodic loading on the blade due to the steady spatial variation of current speeds over the rotor swept area is determined by a limited number of parameters, including tip-speed ratio, Reynolds number, lift and drag coefficients, thrust and torque coefficients, and power coefficient.

1.5 Outline of the thesis

The proposed study is presented in the following six chapters:

Chapter 1 presents a brief background and introduction to the subject area of research.

Chapter 2 provides literature review including the marine current energy resource, resource extraction principles, marine extraction technologies, hydrodynamics and marine current behavior.

Chapter 3 discusses hydrodynamics design of marine current turbines including actuator disc concept, blade element-momentum theory, linear wave theory, basic parameters related to a rotor.

Chapter 4 presents similarity conditions, relevant scaling factors, and numerical investigation of scaling effects.

Chapter 5 presents the results of numerical simulation and prediction of torque, thrust, and bending moments at the root of rotor blades in a horizontal-axis marine current turbine.

Summary, conclusions and future work are presented in **Chapter 6**.

Chapter 2

LITERATURE REVIEW

2.1 Marine Current Energy Resource

Marine currents have great potentials for exploitation of sustainable energy generation if proper methodologies are developed. As with all energy generation developments, this renewable resource has to be well analyzed and understood. The mode of operation for marine current renewable energy technologies is closely related to the nature of its resource as for all other renewable energy resources. Basic understanding of this resource dynamics is of primary importance before exploitation. This chapter seeks to present a brief literature review of the marine current energy resource distribution and estimates for energy production, hydrodynamics and marine current turbine behavior.

2.2 Resource Extraction Principles

Marine current energy conversion concept is different from traditional hydropower conversion where the amount of energy extracted from a river is dependent on the head between the reservoir and the water level below the dam. A similar approach can be used for tidal power in areas with high tides. In that case, a barrage can be constructed in a narrow bay or estuary to utilize the head between the low and high water.

Another way to generate electricity from water would then be to convert the kinetic energy of the flowing water similar to the way a wind turbine would extract energy from the wind. In that case, a dam or reservoir is not necessary; instead sites where the seabed topography and the effect on concentrating the flow caused by coastlines, such as straits and around headlands, causes fast current to occur regularly would be of significant interest. Florida is particularly well endowed with such sites. The velocities needed for potentially cost-effective power generation involve relatively rapid marine currents typically with peak velocities in the region of 2 to 3 m/s (4 to 6 knots) or more. The gross kinetic energy in such flows is extremely large and it appears regularly and predictably. Therefore this is a unique renewable resource that is relatively potent, yet is independent of random weather conditions (Fraenkel, 2002).

2.3 Marine Current Extraction Technologies

The available methods for extracting energy from marine currents are classified into devices that store and release potential energy and those that capture kinetic energy directly. Recent developments for offshore application have concentrated on kinetic energy devices as opposed to the estuary-based storage solution of a tidal barrage. The engineering approach adopted for the development of technology for converting the kinetic energy in marine currents are relatively straightforward and well understood since it follows principles similar to those of a wind turbine. Although there are a large number of devices that have been promoted for extracting energy from fluid flows, it is necessary to use a mechanism which relies primarily on generating torque and hence power from lift forces rather than drag.

As mentioned before, there are only two generic types of kinetic energy conversion rotor that are driven primarily by lift forces and those are the conventional axial flow (propeller) type of rotor also known as horizontal-axis turbine and the cross-flow (Darrieus) rotor known as vertical axis turbine (Figs. 2.1&2.2). The Darrieus type is theoretically just as efficient as the propeller type if the fluid speed is constant, but in practice this efficiency is rarely realized due to the physical stresses and limitations imposed by a practical design and fluid speed variation. Both types of rotor can have fixed blades or variable pitch blades. Whatever type of rotor being used, the theoretical upper limit of efficiency for extracting energy from a free stream (at least where the boundaries are relatively far from the rotor periphery) is 59.3% identified as the Betz's limit, which can be derived from the actuator disk theory (Fraenkel, 2000). The value of the theoretical maximum efficiency is made neglecting the effect of swirl losses at the tips, which is valid for turbines of high tip speed ratio ($\lambda > 3$), wherein

tip speed ratio is defined as: $\lambda = \frac{\Omega R}{U_c}$ (2.1)

where R is the turbine blade radius, Ω the turbine rotational speed, and U_c the current speed.

For turbines with low tip speed ratio ($\lambda=1$) the maximum power coefficient is approximately 42%. The tip speed ratio, λ, is a very important design parameter for the selection of the operation characteristics. The variation of the power efficiency C_p of the turbine with λ determines the operating current velocity range of the turbine, as well as its self-starting capability.

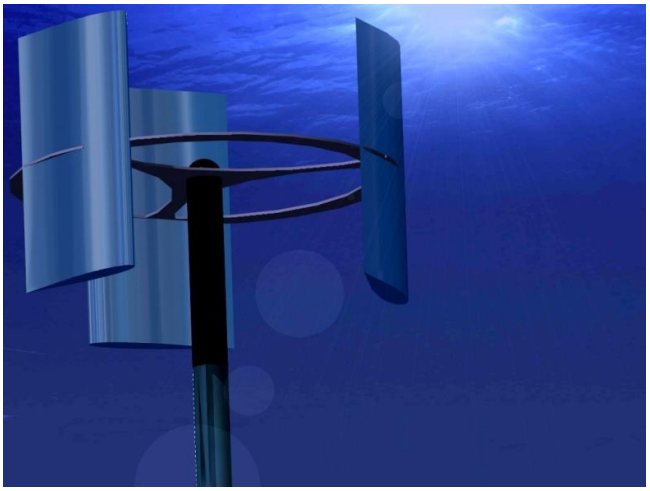

Figure 2.1: Vertical axis marine current turbine (Source: www.esru.strath.ac.uk)

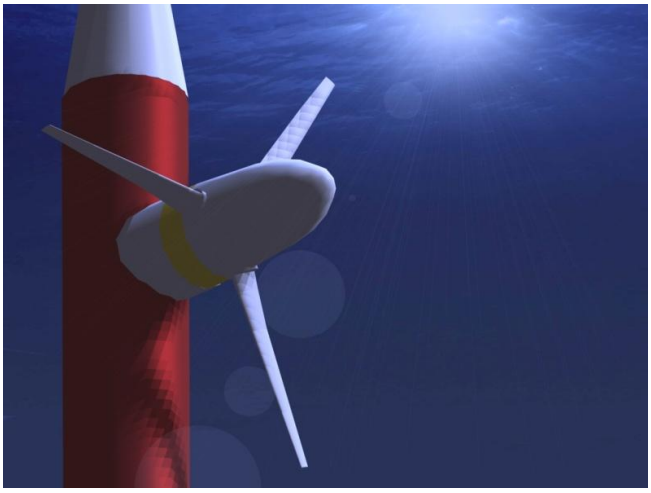

Figure 2.2: Horizontal axis marine current turbine model.
(Courtesy of Marine Current Turbines (MCT) Ltd.)

No published standards are available for this new and fledgling technology. Furthermore, the technology is not mature; many new and sometimes unusual designs are developed and tested. At this stage of development, it is not possible to give full details for a wide range of new devices or even technical data. Since certification needs to be

based on standardized requirements, it is essential to develop guidelines, rules and standards. This has begun in the field of marine current turbines (GL, 2005) and wave energy converters (EMEC, 2004), (DNV, 2004).

As a currently no dedicated standards for all aspects of marine energy converters exist, standards for other technology (wind, oil and gas, maritime,….) have been collected, reviewed and the most appropriate compiled in order to serve as a first basis for design and safety of marine current turbines. Although marine current turbines are novel designs with multiple engineering solutions some parallels can be drawn up to the offshore wind turbines. They are based on the same principle of power extraction. The same hydro- or aerodynamic theories may be applied for analysis. The power output is at the same level and they have a similar machinery design (blades, hub, drive train, electrical installation). The support structure may be of similar design and experiences the same problems regarding soil interaction, scour etc., installation and maintenance may share the same equipment and logistic support.

Due to the nature of marine current turbines and possible interaction with other interests special attention has to be paid during design. The influence of the system on the environment, the safety of human actions at sea transport, fisheries etc., the safety of the persons living in its vicinity and other structures are of considerable interest to engineers. For example, consideration has to be taken for collision prevention, acoustic emissions during operation and installation, and pollution control in case of placement in sensitive areas. Extra risk analysis shall be performed for the tasks mentioned above.

2.5 Marine Current Extraction Systems in Operation or Under Development

Over the last few years, marine energy development has gone through a boost with many prototypes being tested in real coastal sites. The testing of these prototypes helps experts to understand and improve how these devices work in realistic operational conditions. Researchers considered both the level of maintenance and the performance of the system based on numerous experimental simulations. The development of marine current energy technologies is evident in the projects now proposed around the world-300-812 MW in the Korean waters, the Bay of Fundy, Canada (6.6 MW), Paimpol-Behat, France (4 MW), West Bengal, India (4 MW), Pentland Firth, Anglesey, UK (80.5 MW), and Pouto, New Zealand (200 MW). Besides, there are other projects under consideration in the US and Australia. The projected timescales for these projects are within 5 to 10 years. The more advanced proposals typically plan to use variants of Horizontal Axis Tidal Turbines. Although it is suggested that larger powers can be captured with Vertical Axis Tidal Turbines, typically these are less effective at capturing energy for a given swept area (ISSC Committee V.4, 2009).At present, two of the most renowned and successful projects so far developed and installed are SeaFlow and SeaGen by Marine Current Turbines Ltd.

2.5.1 SeaFlow

The first “full-size” marine current turbine known as “SeaFlow” was installed on the North Devon coast, England, in May 2003. It was built by an industrial consortium

consisting of Marine Current Turbines Ltd and several other consultant and manufacturing companies. Financial support for this project was provided by the UK Department of Trade and Industry, the European Commission and German government. SeaFlow's project consists of a horizontal axis marine current turbine with a rotor diameter of 12 m giving a rated power of 300 kW in a current of 2.7 m/s and with a hydrodynamic conversion efficiency consistently exceeding 40%. The rotor is made from composite materials and has a full span pitch control thereby making it capable of generating power for both directions of flow.

Figure 2.3: SeaFlow rotor (Courtesy of Marine Current Turbines (MCT) Ltd.)

2.5.2 SeaGen

SeaGen was installed in Strangford Lough, Northern Ireland in April 2008. It is by far the largest and most powerful tidal turbine in the world with 16 m diameter twin rotors each sweeping over 200 square meters of flow giving an output power of 1.2 MW at current velocity of 2.4 m/s. SeaGen uses axial flow pitched controlled rotors which are the most efficient type of turbine rotors technology of choice in the wind industry. SeaGen's rotors can achieve over 48% efficiency over a broad range of current velocities and they also offer complete control over the machine. The rotors can be shut down in less than three seconds even with the current at full flow.

SeaGen is the intended prototype for widespread commercial technology development with its twin rotors which gives twice the power per pile at significantly less cost. These turbines have a patented feature by which the rotor blades can be pitched through 180^0 in order to allow them to operate in bi-direction flows that is on both the ebb and the flood tides. The twin power units of each system are mounted on wing-like extensions either side of a tubular steel monopole some 3 m in diameter and the complete wing with its power units can be raised above sea level to permit safe and reliable maintenance. Thus far, SeaGen is the largest commercial grid connected machine ever developed in the marine energy industry (Marine Current Turbines Ltd., 2010).

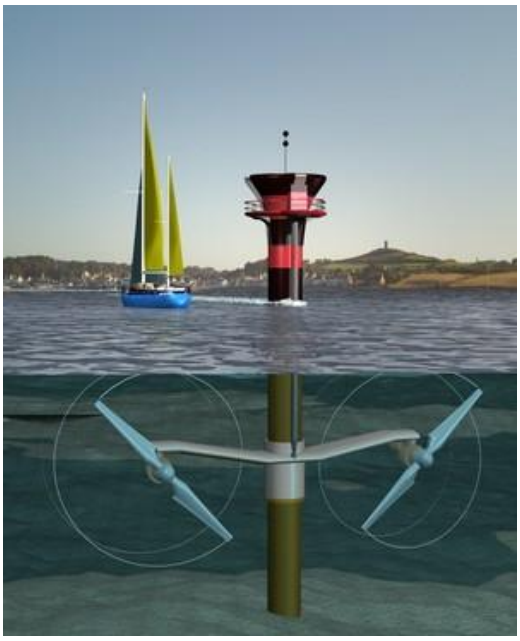

Figure 2.4: SeaGen twin rotor (MCT, 2010)

2.5.3 Grid Connections

As for the integration of marine current turbines into the electricity supply network, one of the main advantages of this technology is the fact that, although tidal cycles are quite complex, they are subject to a predictable schedule, so the power output can be managed and supplied easier and safer than with other renewable energies, where more variability is involved. This is a key factor regarding the future development of tidal energy, as there is the possibility of scheduling the power output and even matching it with local energy demand variation in case some energy storage systems were installed. This would enhance grid stability and contribute to the technical exploitation of marine current turbine farms, boosting their economical viability. However, there is a big issue affecting the wide spread exploitation of this technology, the lack of grid connection

points close to the tidal farms locations. The available connections are likely to be to distribution networks serving small local coastal populations, whose capacity is very limited to take in projects of tens of megawatts if reinforcement modifications are not carried out (Carbon Trust, 2006).

2.5 Resource Estimates and Environmental Impacts

The cost of any given type of energy is a practical way to analyze its technical situation and level of widespread exploitation, and compare it with those from its energy competitors. The cost of tidal energy is basically depending on capital costs, operation and maintenance costs and the amount of electricity produced. As in every technology, the device itself will be economically viable as long as the income produced by the saleable energy is greater than the cost of producing it. The capital cost of a marine current turbine includes mechanical and electrical (including the design and manufacturing process of the rotor and the devices required to output and arrange the mechanical energy into electricity), structural (including the supporting structure as well as its foundation and offshore conditioning) and grid connection (including sub-sea cables and switchgears). The individual contribution to the overall capital cost of these and some others is shown in Fig. 2.5 below:

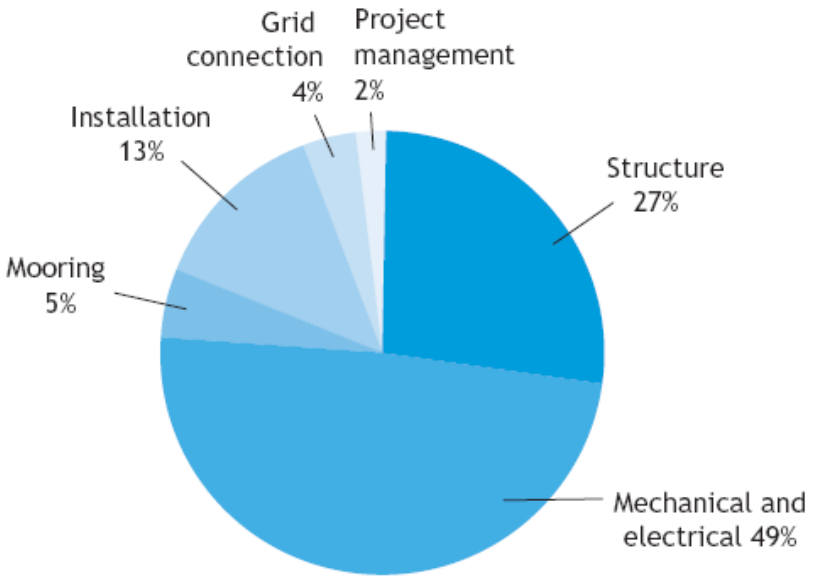

Figure 2.5: Breakdown of capital costs for a tidal stream farm. (Carbon Trust, 2006).

The operation and maintenance cost refers mainly to the cost of both scheduled and unscheduled overhauls, components replacement and monitoring of the device performance. These costs, as well as the capital ones, are highly specific for each site, and they are subject to significant variations to the overall cost depending on the size and location of the tidal farm.

Similar to wind energy, there is big margin in cost reduction as the installed capacity increases, bringing about improvements in technology and more efficient exploitation patterns.

In UK, estimations suggest the cost of energy would have to drop to 7p/kWh by the time 1GW capacity has been installed, as shown in Fig. 2.6 below:

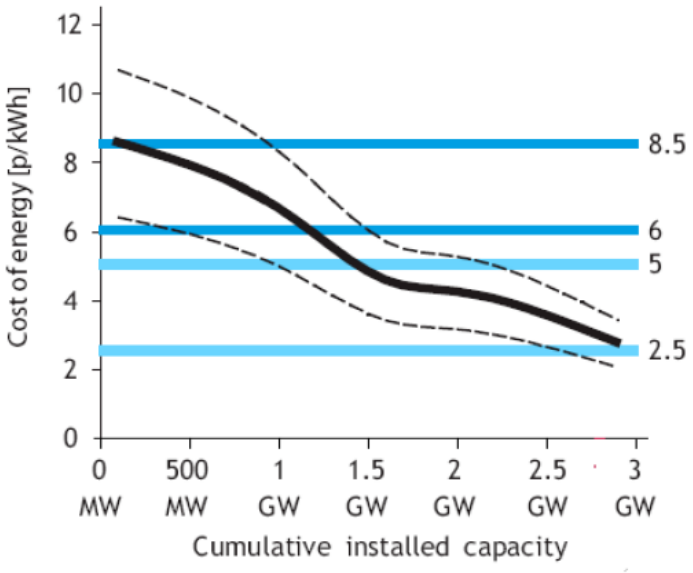

Figure 2.6: UK Tidal stream cost-resource curve (Carbon Trust, 2006).

In the U.S., preliminary estimates of the unit electricity cost from marine current devices vary between 0.045 - 0.135 $/kWh, depending on the device and the assumptions made in the evaluation. An assessment described in the CEC report (1996b) estimated that a cost of less than 0.09 $/kWh would be achievable with first generation machines in a good current regime (current velocity of 3 m/s) with load factor greater than 30% (IEA, 2003).

The environmental impacts of submerged marine current turbines will be low. The main areas of concern are likely to be with regard to navigation and fishing. Generally, marine current power generation is considered environmentally benign. Large-scale installations, whereby the downstream current velocity is altered significantly across the width of an estuary, may have consequences for the transport of sediments and downstream ecosystems. Near-shore and offshore plants may constitute obstacles to

coastal marine traffic and, when deployed in large numbers, may promote modifications to coastal dynamics. Most of these effects can be minimized and, in some cases, eliminated. A detailed environmental impact assessment (EIA) will often be required. A strategy for the assessment and quantification of environmental impacts need to be developed, although the underlying principles of EIA are well developed (IEA, 2003).

2.6 Hydrodynamics

The wave particle kinematics must be determined in order to calculate the hydrodynamic loading on a submerged structure in the time domain. For linear sea states the wave particle velocity and acceleration vectors and dynamic pressure can be calculated using linear Airy wave theory. This theory represents the wave elevation as sinusoid propagating with a constant amplitude and period. For fatigue load calculations in which irregular sea states are required, Airy wave theory can be combined with an appropriate wave energy spectrum in order to create an irregular sea state. Once the wave particle kinematics have been derived, the applied hydrodynamic loads acting on the rotor blades can be divided into a number of elements using the blade element-momentum theory and the total applied load found by integrating the loads acting on each element.

The ability to exploit marine currents sites is dependent on the prediction of the hydrodynamic characteristics. Thus, methodologies need to be established to describe the physical and operational performance of the turbines, allowing designs to be investigated and performance to be evaluated. Batten et *al.* (2007) have investigated the hydrodynamic design of $1/20^{th}$ scale model of a 16 m diameter horizontal axis tidal

turbine in a cavitation tunnel tank. The experiments for different blade pitch settings have been compared with simulations based on a developed blade element-momentum theory. The results include the performance characteristics of the model scale rotor in terms of power, thrust, and cavitation parameters. The cavitation tunnel power coefficient (C_p) measurements show good agreement with the theoretical results for tip speed ratio (TSR) between 3-7. The theory tended to over predict C_p for TSR > 7. The experimental thrust coefficient (C_T) data is validated with numerical simulations and are under predicted by around 5-10% for the 20^o -hub pitch case and 5-15% for the 25^o-hub pitch angles. The authors match the experimental turbine design for a 16 m diameter rotor to a real tidal velocity site data and found that as design speed increases from 2 to 3 m/s there is a slow increase in energy but large increases in maximum thrust. For example, they found that an increase in design TSR from 4 to 5 resulted in over 10% increase in maximum thrust. Such results will have a profound impact on MCT design philosophy and installation costs. The data obtained from this investigation have shown good agreement with published numerical data such as the test program carried out at the Southampton University on model MCT and the developed blade element-momentum theory.

2.7 Marine Current Turbine Behavior

An experimental study was carried out at the French Research Institute for Exploitation of the Sea by Maganga *et al.* (2009) to determine the flow characteristic effects on a 0.70 m diameter marine current turbine. This work focused on studying the behavior of the rotor and characterizing the wake it emitted. The efficiency of the turbine is quantified by the measurement of the thrust and the amount of power generated by the

rotor for various inflow conditions. The turbulence intensity effects on the turbine are also characterized in this work. Two levels of turbulence intensity rates are considered namely 8% and close to 25%. The behavior of the turbine is found to be the same for both types of flow. The thrust fluctuations are always higher for the high turbulence rate than for the smaller one: double for the 25% turbulence intensity rate compared to the 8% rate. The force oscillations are three times greater on the rotor blades due to the level of velocity fluctuation; this could be a useful determinant for the fatigue loading on the structure. The available power for the flow with a turbulence intensity rate of 25% is 15% lower than that of the reference flow.

Myers and Bahaj (2009) studied the flow field around horizontal axis marine current turbines by use of scale mesh disk rotor simulators. This work includes studies of the principal parameters that govern the downstream wake structure and its recovery to the free-stream velocity profile and examined the possibility of installing arrays of devices while maximizing efficiency. The results indicated that wake velocities are reduced in the near wake region for increasing levels of disk thrust and the far wake is a function of the ambient flow turbulence. Variation of the disk proximity to the water surface/bed introduces differential mass flow rates above and below the rotor disk that can cause the wake to persist much further downstream. Turbulent mixing in the boundary region between the wake and the faster moving free stream fluid served to re-energize the wake, breaking it up and increasing the velocity. Devices spaced too closely will suffer a decrease in performance while spacing devices too far apart will lead to a sub-optimal use of surface area within the region of strong tidal flow.

The issues surrounding flow acceleration above and below a rotor within a vertically constrained flow have been addressed to a degree. Longer turbulent length scales in the sea generated wave motion and large changes in bathymetry should serve to reduce the persistence of the wake through greater turbulent mixing in the wake region. Absolute wake lengths and characteristics can be predicted only when the full-scale conditions at marine current energy sites have been accurately quantified.

Recent analysis on the unsteady flow around marine current turbines in yawed flow conditions is presented by Baltazar and Falcao de Campos (2009). The analysis is carried out for axial and yawed inflow conditions for a turbine with controllable pitch settings of 5^o and 10^o in a wide range of tip-speed ratios. The panel method and lifting line calculations were analyzed without and with viscous effects. Corrections in the inviscid lift force and the contribution of section drag force were taken into account. The result showed the inclusion of the viscous corrections is seen to significantly decrease the axial force and power curves, bringing the calculations to a closer agreement with the experimental data, especially for large tip-speed ratios. The authors found the panel method is proven to be a valuable tool for the hydrodynamic analysis of marine current turbines.

Chapter 3

HYDRODYNAMICS OF MARINE CURRENT TURBINES

3.1 Hydrodynamic Design of Marine Current Turbines

The hydrodynamic design parameters for marine current turbine (MCT) entail the choice of diameter, pitch angle and rotational speed. There are major differences in the engineering of a MCT and wind turbines because the density of water is higher compared with air; thus marine current turbine can be of much smaller diameter and rotate at lower speeds. Horizontal axis marine current turbine blades are significantly smaller than those of horizontal axis wind turbine (HAWT), 3 to 22 m in diameter compared to 30 to over 100 m in diameter. Also, the rotor diameter of a MCT does not need to be as large as a HAWT to produce same amounts of power due to the large density difference between air and water. Water with greater density than air yields high energy densities at low velocities, but it also yields correspondingly large forces on the rotor structure compared with a wind turbine. However, the success of using marine current turbines to tap the marine currents is partly dependent on predicting their hydrodynamic characteristics. Consequently, methodologies are needed to describe the physical and operational performance of the turbines. This does not only allow appropriate designs to be investigated and performance evaluated but also provide long-range forecasting for

energy yields of such turbines. Therefore, careful attention must be paid to the analysis and simulation of the hydrodynamic forces on the marine current turbine rotor blades (Batten et al.; 2006 and 2007).

A methodology is presented for the hydrodynamic design of horizontal axis marine current turbines (Molland *et al*., 2005). The performance of suitable 2D section shapes was investigated both experimentally in a cavitation tunnel and with numerical simulations. A numerical model of a typical 3D rotor is used to demonstrate parametric variations of the design parameters and the use of alternative blade section. This investigation demonstrates how blade pitch angle or changes in camber alter stall performance and delay the possibility of cavitation for marine current turbine.

Tidal Generation Limited (TGL) developed a 500 kW fully submerged tidal turbine. The performance characteristics of a scale model tri-bladed horizontal axis turbine of a 500 kW were evaluated in a free surface circulation tank (Maganga *et al*., 2009). The pitch-controlled scale model had a diameter of 0.6 m, tested at speeds ranging from 0.5 to 1.5 m/s , and its performances were obtained over a range of rotor speeds from 10 to 190 rpm and blade pitch angle from -5 to 15 degrees. Two power control strategies were also tested to investigate the sensitivity of the turbine power output to natural turbulent fluctuations in the flow. The data from the model was used in the design of the control system for the large scale 500 kW machine minimizing the fluctuations in rotor torque. This type of turbine is not sensitive to the quality of the incoming flow, but a misalignment of a fixed turbine can cause a significant loss of

power. The study recommends further research simulating more realistic sea states (wave effects) and combined trials with wave and current interactions on the marine current turbine.

Experimental verifications of two numerical predictions codes based on blade element momentum theory are conducted in (Bahaj et al., 2007) for the hydrodynamic performance of horizontal axis marine current turbines. This study reports on the development and verification of two simulation tools, a commercial code (GH-Tidal Bladed) and an academic in-house code (SERG-Tidal), from experimental measurements conducted on a model 800 mm diameter turbine in a cavitation tunnel and a towing tank. The results of the two codes are compared. These results indicate that the two developed codes demonstrate similar trends in the results and provide a satisfactory representation of the experimental turbine performance .The experimental data includes measurements of shaft power and thrust generated by the turbine for a series of blade pitch settings and speeds. The analysis established that the comparison of the experimental results shows the applicability of using a towing tank with appropriate corrections. The accuracy of the predictions is satisfactory for using the developed theoretical tools for design exercises and parametric studies. In general, for off-design cases, GH-Tidal Bladed code tended to slightly over estimate the power while SERG-Tidal code underestimated the thrust. The results of this study indicate the usefulness of developing tools for this new technology; and similar to wind turbines, these tools are likely to aid in the understanding of design and performance characteristics of marine current turbines.

3.2 Actuator Disc Concept

The mechanics of rotor power absorption from marine currents begins with an analysis of the hydrodynamic behavior of the rotor by considering the energy extraction process. The rotor is replaced by an "actuator disc" through which the static pressure decreases discontinuously (Fig. 3.1). The assumptions on which the actuator disc theory are based on:

1. Steady, homogenous flow.
2. No obstructions to current flow either upstream or downstream
3. Uniform flow velocity at disc or assume uniform thrust loading on the disc
4. Current flow passing through the disc separable from remaining flow by well-defined streamtube
5. Current flow incompressible
6. No rotation of flow produced by disc

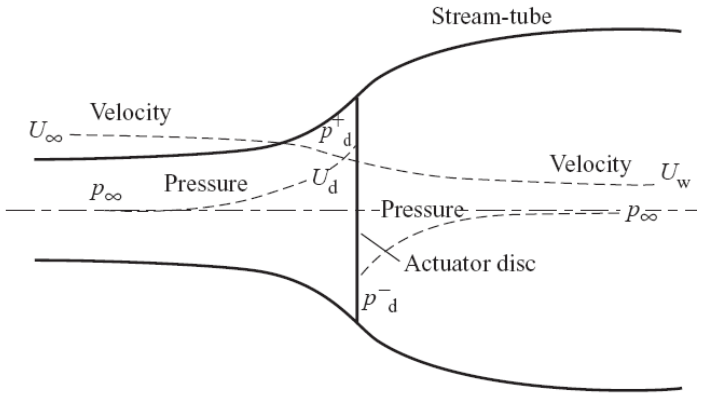

Figure 3.1: An Energy Extracting Actuator Disc and Stream-tube (Burton et al., 2001).

Upstream of the disc the stream-tube has a cross sectional area smaller than that of the disc and an area larger than the disc downstream. The expansion of the stream-tube is because of the mass flow rate must be the same everywhere. The mass flow which passes through a given cross section of the stream-tube in a unit length of time is ρAU, where ρ is the fluid density, A is the cross-sectional area and U is the flow velocity. The mass flow rate is uniform along the stream-tube and hence,

$$\rho A_\infty U_\infty = \rho A_d U_d = \rho A_w U_w \tag{3.1}$$

The symbol ∞ refers to conditions far upstream, d refers to conditions at the disc and w refers to conditions in the far wake.

The actuator disc induces a velocity variation which must be superimposed on the free stream velocity. The stream-wise component of this induced flow at the disc is given by $-aU_\infty$, where a is called the axial flow induction factor. The net stream-wise velocity at the disc is

$$U_d = U_\infty(1 - a) \tag{3.2}$$

The marine current turbine is a lift dependent device. The theoretical procedure used in this study is based on the classical blade element-momentum theory combined with linear wave theory to predict the hydrodynamic loads on the rotor blades. Even though the engineering principles are similar to horizontal axis wind turbine corrections are necessary to account for the effects of free surface, viscosity, and possible occurrence of cavitation.

3.3 Blade Element Theory

The blade element theory is used to simulate the torque, thrust, and bending moments induced by the detailed stream flows along the rotor blades. It also provides basic insights into the rotor performance as well as the estimate of the lift and drag forces at the strip using the 2-D aerofoil characteristics of the section. The forces on the blade element are shown in Fig. 3.2. By definition the lift and drag forces are perpendicular and parallel to the incoming flow, respectively. Each blade of the marine current turbine is divided into 16 elements. Lift and drag coefficients are then calculated as functions of incident angles and adjusted to account for 3-D effects. Velocities of the flow passing the blade element are computed considering the wave-current interactions. Directional components of these velocities consist of out-of-plane and in-plane velocities. Using the directional components of the velocities, the out-of-plane and in-plane lift and drag forces are calculated on the blade section.

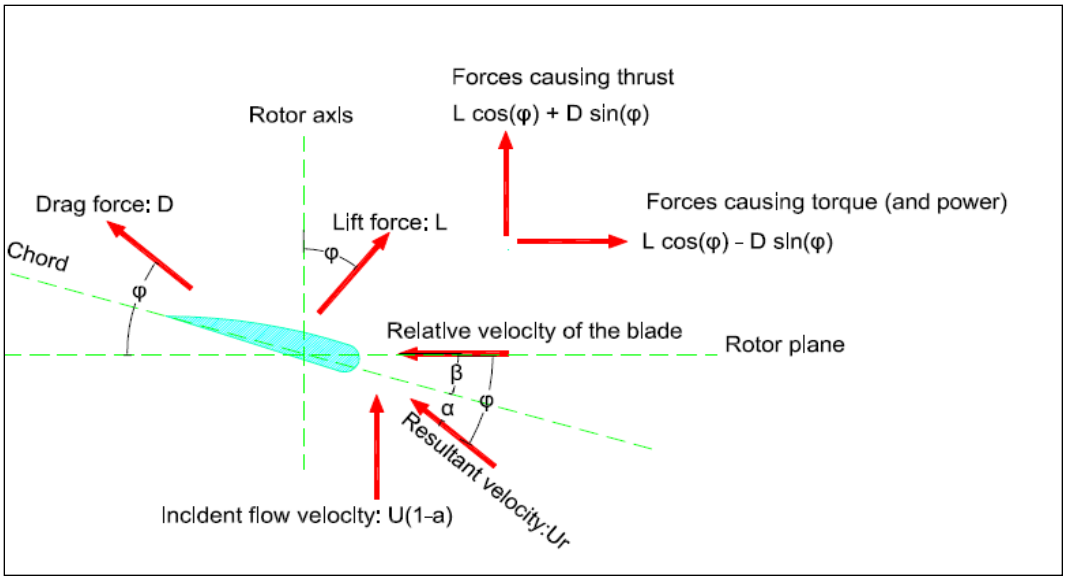

Figure 3.2 : Lift and drag forces resolved into in-plane (torque) and out-of- plane (thrust) directions on a blade cross-section.

From Figure 3.2, the resultant relative velocity at the blade is

$$U_r = \sqrt{U^2(1-a)^2 + \Omega^2 r^2(1+a')^2} \tag{3.3}$$

Which acts at an angle φ to the plane of rotation, such that

$$sin\varphi = \frac{U(1-a)}{U_r} \tag{3.4a}$$

and

$$cos\varphi = \frac{\Omega r(1+a')}{U_r} \tag{3.4b}$$

where $\Omega r(1+a')$ is the net tangential velocity experienced by the blade element and $U(1-a)$ is the incident flow velocity.

The angle of attack α is given by

$$\alpha = \varphi - \beta \tag{3.5}$$

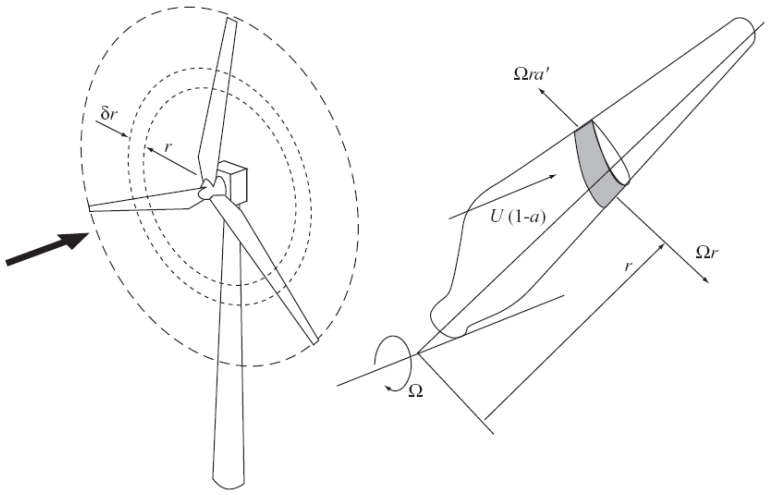

Figure 3.3: A Blade Element Sweeps Out an Annular Ring (Burton et al., 2001).

Figure 3.3 shows the tangential velocity of the blade element combined with the tangential velocity of the wake $a'\Omega r$.The lift force on a span-wise length δr of each blade, normal to the direction of U_r, is therefore

$$\delta L = \frac{1}{2}\rho {U_r}^2 cC\delta r \qquad (3.6)$$

And, the drag force parallel to U_r is

$$\delta D = \frac{1}{2}\rho {U_r}^2 cC_d r\delta r \qquad (3.7)$$

3.4 Blade Element-Momentum (BEM) Theory

The vast majority of aeroelastic wind turbine simulation code used the combined blade element and momentum (BEM) theory to model aerodynamic forces acting on a wind turbine rotor. This method was developed from the helicopter aerodynamics. Due to its convenience and reliability, this method is the most widely-used for calculating the

aerodynamic forces on wind turbines. Marine current turbine (MCT) design codes are no exception and BEM theory is used in all MCT hydrodynamic performance analysis.

BEM theory models the rotor as an actuator disc assuming axis-symmetric, incompressible, steady flow in a stream tube. The power extracted by the rotor and the thrust force acting on the rotor can be derived using Bernoulli's theorem, which assumes that the balances between changes in momentum and energy flow rates are conserved. Momentum theory can then be applied on annular level to match the results of momentum analysis with the blade element properties and geometry. The force in a blade element is assumed to be solely responsible for the change of momentum of the fluid which passes through the annulus swept by the element.

Determination of rotor forces and power using BEM theory

The component of force on *N* blade elements resolved in the axial direction is

$$\delta L cos\varphi + \delta D sin\varphi = \frac{1}{2}\rho {U_r}^2 Nc(C_L cos\varphi + C_d sin\varphi)\delta r \qquad (3.8)$$

The rate of change of axial momentum of the air passing through the annulus is

$$\rho U(1-a)2\pi r\delta r 2aU = 4\pi\rho U^2 a(1-a)r\delta r \qquad (3.9)$$

The drop in wake pressure caused by wake rotation is equal to the increase in dynamic head and given by

$$\frac{1}{2}\rho(2a'\Omega r)^2 \qquad (3.10)$$

Therefore, the additional axial force on the annulus is

$$\frac{1}{2}\rho(2a'\Omega r)^2 2\pi r\delta r \tag{3.11}$$

Thus

$$\frac{1}{2}\rho {U_r}^2 Nc(C_L cos\varphi + C_d sin\varphi)\delta r = 4\pi\rho[U^2 a(1-a) + (a'\Omega r)^2]r\delta r \tag{3.12}$$

Simplifying,

$$\frac{W^2}{U_\infty^2} N\frac{c}{R}(C_L cos\varphi + C_d sin\varphi) = 8\pi(a(1-a) + (a'\lambda\mu)^2)\mu \tag{3.13}$$

The element of axial rotor torque caused by the fluid forces on the blade elements is

$$(\delta L sin\varphi - \delta D cos\varphi)r = \frac{1}{2}\rho {U_r}^2 Nc(C_L sin\varphi - C_d cos\varphi)\delta r \tag{3.14}$$

The rate of change of angular momentum of the fluid passing through the annulus is

$$\rho U(1-a)\Omega r 2a'r 2\pi r\delta r = 4\pi\rho U(\Omega r)a'(1-a)r^2\delta r \tag{3.15}$$

Equating the two moments

$$\frac{1}{2}\rho {U_r}^2 Nc(C_L sin\varphi - C_d cos\varphi)\delta r = 4\pi\rho U(\Omega r)a'(1-a)r^2\delta r \tag{3.16}$$

Simplifying,

$$\frac{U_r^2}{U^2} N\frac{c}{R}(C_L sin\varphi - C_d cos\varphi) = 8\pi\lambda\mu^2 a'(1-a) \tag{3.17a}$$

where the parameter $\mu = {}^{r}/_{R}$

It is convenient to express

$$C_L cos\varphi + C_d sin\varphi = C_x \text{ and } C_L sin\varphi - C_d cos\varphi = C_y \tag{3.17b}$$

Equations 3.13 and 3.17a are solved by an iterative process for the flow induction factors, a and a', at each radius, in terms of the flow angle, φ

$$\frac{a}{1-a} = \frac{\sigma_r}{4sin\varphi^2}[(C_x) - \frac{\sigma_r}{4sin^2\varphi}C_y^2] \tag{3.18}$$

$$\frac{a}{1+a'} = \frac{\sigma_r C_y}{4sin\varphi cos\varphi} \tag{3.19}$$

The solution for flow induction factors is usually carried out iteratively because the two- dimensional aerofoil characteristics are non-linear functions of the angle of attack. The iterative procedure is significant in determining the complete performance characteristics of a rotor. Initially, it begins by assuming a and a' to be zero, in determining φ , C_p and C_d and then calculate the new values for the flow induction factors using the Equations 3.18 and 3.19. The iteration is repeated until convergence is achieved.

Blade solidity σ is defined as total blade area divided by the rotor disc area and is a primary parameter in determining rotor performance. Chord solidity σ_r is defined as the total blade chord length at a given radius divided by the circumferential length at that radius.

$$\sigma_r = \frac{N}{2\pi}\frac{c}{r} = \frac{N}{2\pi\mu}\frac{c}{R} \tag{3.20}$$

The torque developed by the blade elements of span-wise length δr is given by

$$\delta Q = 4\pi\rho U(\Omega r)a'(1-a)r^2\delta r \tag{3.21}$$

If drag, or part of drag, has been excluded from the determination of the flow induction factors then its effect must be introduced when the torque caused by drag is calculated from blade element forces,

$$\delta Q = 4\pi\rho U(\Omega r)a'(1-a)r^2\delta r - \frac{1}{2}\rho {U_r}^2 NcC_d \cos(\varphi)\, r\delta r \tag{3.22}$$

The complete rotor, therefore, develops a total torque Q:

$$Q = \frac{1}{2}\rho U^2 \pi R^3 \lambda \left[\int_0^R \mu^2 \left[8a'(1-a)\mu - \frac{U_r}{U}\frac{N\frac{c}{R}}{\pi}C_d(1+a')\right]d\mu\right] \tag{3.23}$$

The power developed by the rotor can be obtained by

$$P = Q\Omega \tag{3.24}$$

Simple BEM theory is very rarely used in isolation, as it does not deal with the unsteady nature of the forces by a turbine rotor blade. Therefore, there are a number of corrections commonly applied in conjunction with the BEM method to account for this. The most common corrections applied to the quasi-steady momentum theory are blade tip and root effects, turbulent wake effect, wake state, dynamic inflow, dynamic stall, and 3-D corrections. Although the BEM theory is well established and widely used, it is significant to have experimental verification of its modified version for marine current turbine rotor analysis.

The first correction is the inclusion of tip and hub loss factors in the BEM equations. The tip and hub loss factors account for the fact that the axial flow induction factor *a* is not uniform over the rotor area but fluctuates between the passing of each blade, with the overall effect of reducing the net power extracted. This fluctuation is due

to the vorticity distribution in the wake arising from the finite number of blades. At the blade root and blade tip the bound circulation around the aerofoil must reduce to zero resulting in a vortex being trailed into the rotor wake resulting in the losses.

For example, the following loss is not accounted for by the BEM theory and is being considered in the numerical simulation:

Tip loss

Using Prandtl's analysis (Fig.3.4), the tip loss factor can be obtained from

$$f(r) = \frac{2}{\pi}\cos^{-1}[e^{-\pi(R_w/d - r/d)}] \tag{3.25}$$

where $f(r)$ is the tip-loss function which has a value less than unity and equal to zero at the wake boundary. $R_w - r$ is the distance measured from the wake edge, with R_w being the wake radius and r is a radius to any line parallel to the rotor axis, somewhat smaller than the wake radius (rotor radius). The distance d is taken as the normal distance between successive helicoidal vortex sheets (MCT Ltd., 2010).

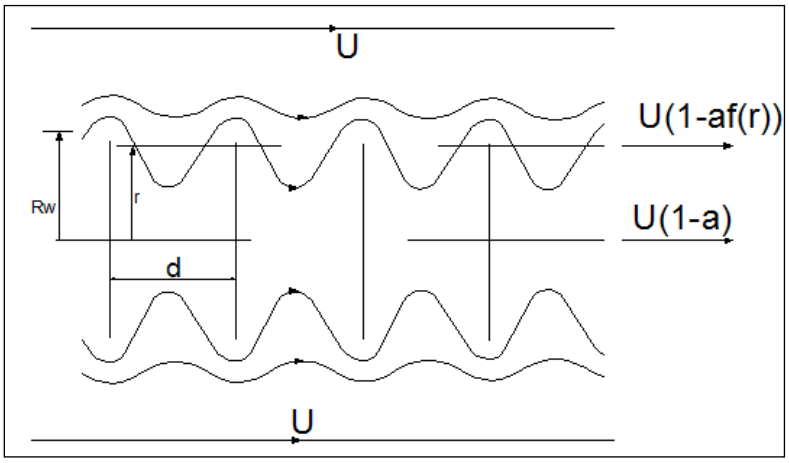

Figure 3.4: Prandlt's Wake-disc Model to account for Tip-losses (Burton et al., 2001).

3.5 Linear Wave Theory

Before embarking on the analysis of linear waves, it is important to consider the physical properties of a traveling surface wave. Figure 3.5 shows the origin of the Cartesian coordinate system is on the SWL, which is the calm-water position. The water depth, *h*, is measured from the sea floor to the SWL. The wave has a height, *H* (measured from the trough to crest), and a wave length, λ, (measured from crest to crest), and travels in the *x*-direction at a celerity, *c*. the vertical free surface displacement, η(*x*,*t*), is measured from the SWL and, as indicated, is a function of both time, *t*, and distance, *x*.

Linear wave theory is based on linearization of the boundary conditions at the air-water interface. The equation for the horizontal and vertical velocities of a particle at any mean depth $-z$ below the still water level is determined from $\partial\phi/\partial x$ and $\partial\phi/\partial z$ respectively, where ϕ is the velocity potential and $u=\partial\phi/\partial x$ and $v=\partial\phi/\partial z$. The particle horizontal, ξ, and vertical, ζ, displacements about a fixed point (x_o, z_o) are derived by integrating the respective velocities over the wave period (Fig.3.5). The resulting equations are given by,

$$\xi = -\frac{H}{2}\frac{\cosh[k(z_o+h)]}{\sinh(kh)}\sin(kx_o - \omega t) \tag{3.26}$$

$$\zeta = \frac{H}{2}\frac{\sinh[k(z_o+h)]}{2\sinh(kh)}\cos(kx_o - \omega t) \tag{3.27}$$

The location vector of the particle from the mean position is given by,

$$\bar{r} = \xi\bar{\imath} + \zeta\bar{k} \tag{3.28}$$

$$\bar{r} = \frac{\frac{H}{2}}{\sinh(kh)}\{-\cosh[k(z_o+h)]\sin(kx_o - \omega t)\,\bar{\imath} + \sinh[k(z_o+h)]\cos(kx_o - \omega t)\bar{k} \tag{3.29}$$

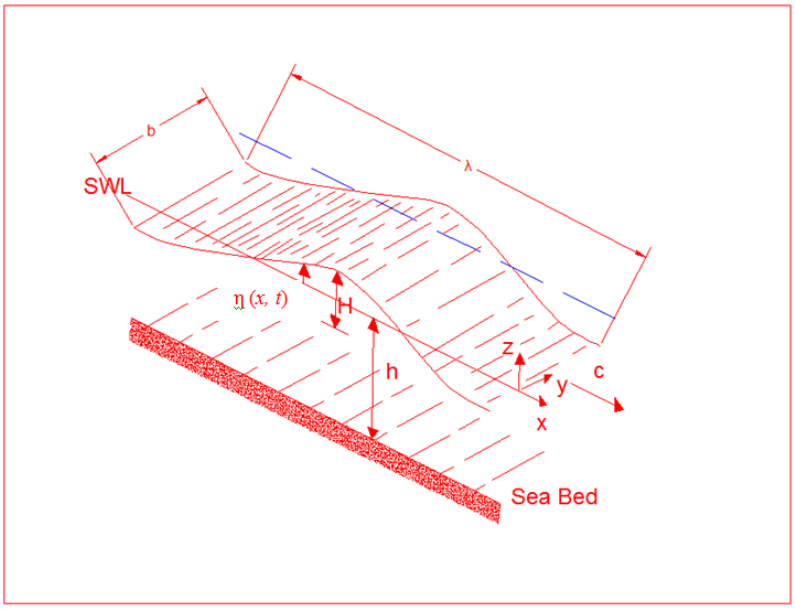

Figure 3.5: Sketch and Notation for the Linear Wave Analysis (McCormick, 2010).

The waves can cause change of flow velocity field and pressure field around the marine current turbine rotor. The change in the flow velocity field will affect the fluid forces on the rotor. The changes in the flow velocity field and pressure field may initiate or reduce the occurrence of cavitation. The magnitude and direction of the velocity induced by the waves will have an effect on the rotor. The horizontal particle velocity on the rotor is given by,

$$u = \frac{\pi H}{T_w} \frac{\cosh[k_w((zr - d_s) + d)]}{\sinh(k_w d)} \cos(\alpha_w) \tag{3.30}$$

This horizontal wave particle velocity will increase the incident flow velocity, if both velocities are in the same direction or decrease the flow velocity, if they are not in the same direction.

Vertical wave particle velocity is given by,

$$v = \frac{\pi H}{T_w} \frac{\sinh[k_w((zr - d_s) + d)]}{\sinh(k_w d)} \sin(\alpha_w) \tag{3.31}$$

where,

H= wave height

d_s= rotor axis depth

d= water depth

k_w= wave number

T_w= wave period

z_r= instantaneous vertical position of centroid of blade

section with respect to rotor axis

This vertical velocity of the particle will change the flow incidence angle and hence modify the lift and drag forces.

Since the current alters the wave celerity, the encountered wave frequency becomes

$$f_e = \frac{1}{T_c} = \frac{1}{T_w} + \frac{U_c}{L_w} \cos(\theta_w) \tag{3.32}$$

where U_c is the current velocity, T and L are wave period and length, respectively. Subscripts 'c', 'e' and 'w' represent current, encountered, and wave, respectively. θ is the incident angle of the current.

3.6 Two-dimensional Aerofoil Theory

As air flows past an aerofoil, it generates both normal pressure and shear stresses at every point when the air touches the foil. The total forces on an aerofoil can be determined by integrating these pressures and stresses over the surface of the aerofoil. Any set of forces on a rigid body can be resolved about an arbitrary point into two perpendicular forces and one moment. For aerofoil, the general convention is that the drag force, *D*, is measured in the direction of the free-stream relative wind felt by the aerofoil. The lift force, *L*, is measured perpendicular to this relative wind. The aerodynamic moment is usually measured about 25 % chord point i.e. one fourth of the way back from the leading edge of the foil on the line joining the leading and trailing edges. The length of *c* is called the chord of the foil and the conventions are shown in Fig. 3.6.

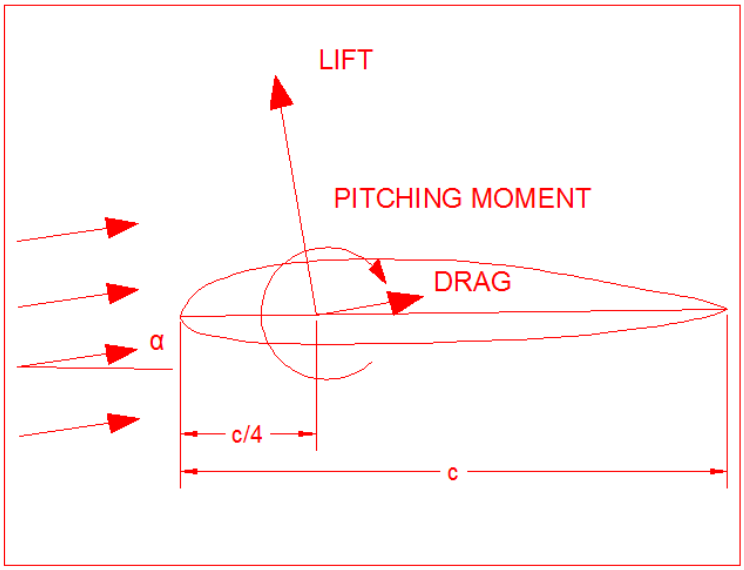

Figure 3.6 : Aerodynamic forces and moment.

Based on the results of published experimental work in two-dimensional flow, the lift force, *L*, and drag force, *D*, together with the moment on an aerofoil, *M*, are given in standard dimensionless ratios- c_l, c_d and c_m as shown in the following equations:

Lift coefficient, c_l, is given by

$$c_l = \frac{Lift}{\frac{1}{2}\rho U^2 A} \tag{3.33}$$

Drag coefficient, c_d, is expressed by

$$c_d = \frac{Drag}{\frac{1}{2}\rho U^2 A} \tag{3.34}$$

Moment coefficient is computed from

$$c_m = \frac{Moment}{\frac{1}{2}\rho U^2 Ac} \tag{3.35}$$

Power that can be extracted from a stream of water is determined from

$$P = \frac{1}{2} C_p \rho U_\infty^3 A \tag{3.36}$$

where ρ is the density of water, A is the cross-sectional area of the rotor, c is the blade chord, C_p is the power coefficient, and U is the free-stream velocity of the current.

The lift, drag and moment coefficients are given as functions of the angle of attack, α,

which is the angle from the direction of flow to the aerofoil chord length. This angle is given (Fig. 3.1) by

$$\alpha = \phi - \beta \tag{3.37}$$

where ϕ is the flow angle of resultant velocity U_r to rotor plane and pitch angle β is measured between the aerofoil zero lift line and the plane of the disc.

The power developed by the rotor is $P = Q\Omega$.

Where

Q = total torque

Ω = blade angular velocity

The efficiency of a rotor's power extraction is commonly reflected through its power coefficient defined as

$$C_p = \frac{P}{\frac{1}{2}\rho U_\infty^3 A} = \frac{16nQ}{\rho U_\infty^3 D^2} \tag{3.38}$$

A typical performance curve for a modern high speed wind turbine is shown in Fig. 3.7.

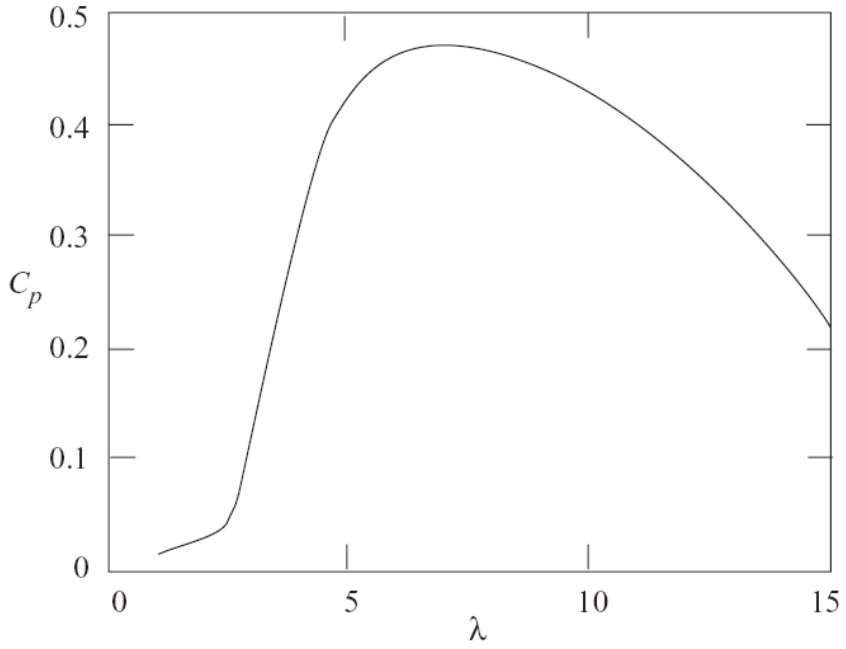

Figure 3.7 : Power Coefficient - Tip Speed Ratio Performance Curve (Burton et al., 2001)

The thrust coefficient is the non-dimensional coefficient used to measure the dynamic force imposed on the rotor along the shaft and is given by

$$C_T = \frac{T}{\frac{1}{2}\rho U_\infty^2 A} = \frac{8T}{\rho \pi D^2 U_\infty^2} \qquad (3.39)$$

where T is the thrust of the rotor.

For the operation of marine current turbine, Reynolds number is an important parameter as it affects the lift, drag, and cavitation characteristics of the rotor. The Reynolds number is given by

$$\mathrm{Re} = \frac{\sqrt{U_c^2 + (0.7D\pi n)^2}}{\nu} C_{0.7R} \qquad (3.40)$$

where $C_{0.7R}$ is the blade chord length at 0.7R radius, U_c is the current speed, n is the rotational speed (rev/s), D is the diameter of rotor, and ν is the kinematic viscosity of water at 20°C.

In the numerical simulations presented in this study, the Reynolds number varies in the range of 0.75×10^6 to 1.5×10^6 for S814 air foil data. A low Reynolds number can degrade the dynamical properties of the aerofoil.

Tip-speed ratio is a characteristic parameter that differentiates the marine current rotor turbine from a ship's propeller. Higher tip speed ratio results in higher noise levels and requires stronger blades due to large centripetal forces. The tip-speed ratio, λ, is defined as the ratio between the tangential speed, ΩR, at the tip of the rotating blade to the current speed, U_c.

$$\lambda = \frac{\Omega R}{U_c} = \frac{2\pi n R}{U_c} \qquad (3.41)$$

The thrust on the rotor can be determined from

$$T = \frac{1}{2}\rho A\,(U_\infty^2 - u_1^2) \qquad (3.42)$$

where

u_1 = fluid velocity downstream beyond the disc plane (Fig. 3.8).

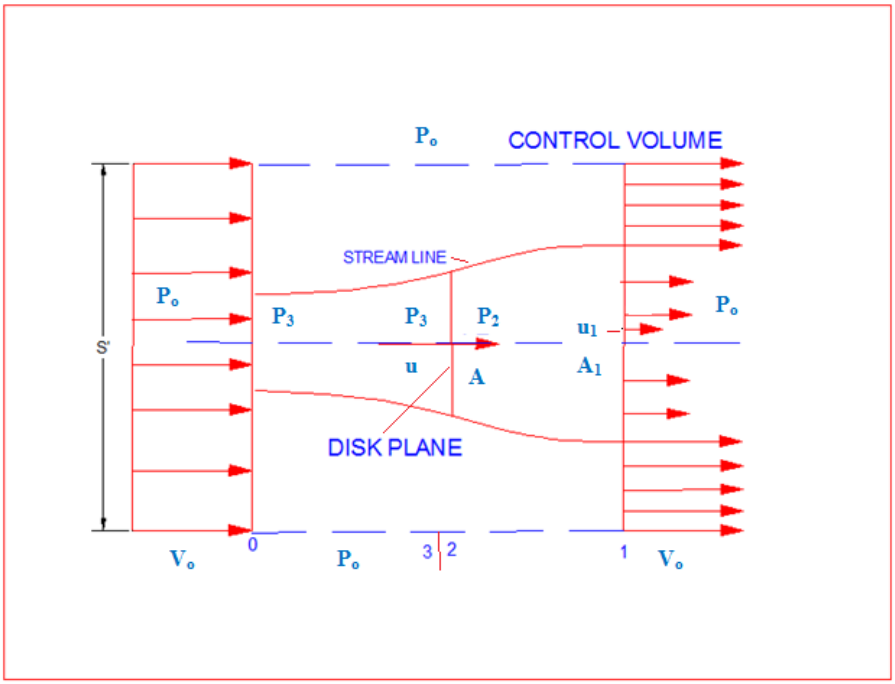

Figure 3.8: Flow pattern (Eggleston and Stoddard, 1987)

Consider the flow diagram for a cylindrical control volume of cross-sectional area *S* and note stations 0, 3, 2, and 1. The flow approaches the rotor at velocity $V_o = U_\infty$ far upstream at station 0 at static pressure P_o. Energy is extracted by the rotor, and the reduced velocity causes the streamline to expand. If the velocity decrease induced by the rotor is v , then the velocity at the disc is $V_o - v = u$, while far downstream at station 1 the flow has been slowed to velocity u_1 and the pressure has returned to P_o. Let A be the area of the rotor at the disc and ρ be the fluid density. The momentum loss of the fluid is the result of the thrust T that rotor exerts against the flow, combined with the net resultant of the external pressure on the control volume as shown in Fig. 3.8. Since the static atmospheric pressure, P_o, acts on the entire volume, its net resultant is zero.

Chapter 4

DYNAMIC HYDROELASTIC SCALING OF MARINE ROTORS

4.1 Introduction

In recent years, there has been an increased interest in the use of composite materials in renewable energy applications. Compared to metals, composites offer the advantages of higher strength-to-weight and stiffness-to-weight ratios, better fatigue characteristics, lower life-cycle cost, and the ability to be tailored to improve structural performance. However, care must be taken when designing such composite rotors in order to avoid aeoroelastic or hydroelastic instability failures, excessive deformations, or problems related to operation or power control. Considering the interests in development of large-scale, energy-efficient composite marine turbines, it is crucial to understand the scaling relationships to properly design and interpret model-scale studies. Both experimental and numerical data for model-scale studies are well established for wind energy and marine applications.

Although these successes have been demonstrated via model-scale experimental and numerical studies, more work is needed to demonstrate similar performance for full-scale composite marine current turbines. Hence, hydrodynamic scaling relationships must

be established to properly represent the dynamic behavior of the prototype. To apply the data for model-scale studies to full-scale analysis, certain similitude conditions such as geometric configurations, kinematic similarity, and dynamic similarity must be met. This chapter presents the similarity relationships for the marine composite rotors (Young, 2010).

4.2 Similarity Conditions

For geometric similarity to be established, the model and full-scale turbines must have the same shape as well as all linear dimensions must have the same ratios to reproduce the same hydrodynamics, including cavitation inception speed and cavitation patterns.

Composite marine current rotors are purposely designed such that the bending and twisting deformations induced by the hydrodynamic load are used to passively adjust the three dimensional (3D) blade deformations to improve the rotor performance. Thus, it is necessary to preserve the same 3D deformation patterns and same load-deformation behavior such that the current/wave-structure interaction response is the same for the model and the prototype. The normalized variation of *EI, GJ,* and *K* along the radial direction must be the same as the prototype for a geometrically similar model. In addition, the ratio of the elastic bending force to fluid inertial force (α_E), the ratio of the elastic torsional rigidity (α_{BT}), and the ratio of the elastic bending –twisting coupling

rigidity to elastic bending (α_C) must all be the same between the model and the prototype to achieve the same 3D deformation effects and load-deformation relationships.

Kinematic similarity must also be established by means of similarity of velocities. Thus the flow will have geometrically similar motions in the model and full scale. For example, the velocities in *x* and *y* direction must have the same ratio, so that a circular motion in full scale must be a circular motion also in the model scale. Also the ratio between rotor tip speeds must be the same for both the model and the prototype and it is governed by,

$$J_F=J_M \rightarrow \frac{V_F}{n_F\, D_F} = \frac{V_M}{n_M\, D_M} \qquad (4.1)$$

Dynamic similarity can be established if the ratios between forces in full scale are the same in model scale. It also requires that cavitation is correctly modeled by equality in the cavitation number, σ, given by

$$\sigma = \frac{(\rho g h + p_0) - p_v}{0.5 \rho U^2} \qquad (4.2)$$

where:

P_0= atmospheric pressure

P_v= vapor pressure

ρgh= hydrostatic pressure

The following force contributions are of importance:

- Inertia forces, F_i
- Viscous forces, F_v
- Gravitational forces, F_g
- Pressure forces, F_p
- Elastic forces in the fluid (compressibility), F_e.
- Surface forces, F_s.

One important consideration is that the dominant forces acting on the model should have the same scale. For a flexible composite rotor operating in a spatially non-uniform flow field, the following principal forces need to be considered:

- Elastic force: $F_E \alpha ED^2$
- Gravitational force: $F_G \alpha \rho_s gD^3$
- Hydrodynamic inertia force (including fluid structure interaction effects): $F_H \alpha \rho n^2 D^4$
- Rotor (centrifugal and oscillatory) inertia force: $F_I \alpha \rho_s n^2 D^4$

The 12 independent variables that affect a rotor performance are listed in Table 1. The effects of surface waves, yaw, and shaft inclination angles of the rotor are ignored in Table 4.1 for simplicity.

Table 4.1: Independent variables that influence a rotor performance.

Variable	Symbol	Dimensions
Fluid density	ρ	ML^{-3}
Fluid kinematic viscosity	ν	$L^2 T^{-1}$
Speed of sound in the fluid	a	LT^{-1}
Saturated liquid vapor pressure	P_v	$ML^{-1} T^{-2}$
Gravitational acceleration	g	LT^{-2}
Mean axial inflow/advance velocity	V	LT^{-1}
Rotor diameter	D=2R	L
Rotor angular velocity	Ω=2πn	T^{-1}
Effective structural density	ρ	ML^{-3}
Effective bending rigidity	EI	$ML^3 T^{-2}$
Effective torsional rigidity	GJ	$ML^3 T^{-2}$
Effective bending-twisting coupling rigidity	K	$ML^3 T^{-2}$

The 12 independent variables listed in Table 1 can be reduced to the following nine non-dimensional parameters that govern the rotor performance:

$$J = \frac{V}{nD} = \text{advance coefficient } \alpha \ \frac{\text{mean axial flow velocity}}{\text{tip tangential flow velocity}} \tag{4.3}$$

$$\sigma_n = \frac{P - P_v}{0.5\rho n^2 D^2} = \text{Cavitation number } \alpha \ \frac{\text{fluid pressure energy}}{\text{fluid kinetic energy}} \tag{4.4}$$

$$\alpha_E = \frac{E}{\rho n^2 D^2} = \text{Elasticity ratio } \alpha \frac{\text{elastic bending force}}{\text{fluid inertia force}} \quad (4.5)$$

$$\alpha_{BT} = \frac{GJ}{EI} = \text{Torsion to bending rigidity ratio} \quad (4.6)$$

$$\alpha_C = \frac{K}{EI} = \text{Bending} - \text{twisting coupling ratio} \quad (4.7)$$

$$\alpha_\rho = \frac{\rho}{\rho_s} = \text{Density ratio } \alpha \frac{\text{fluid inertial force}}{\text{rotor inertial force}} \quad (4.8)$$

$$F_n = \frac{n^2 D}{g} = \text{Froude number } \alpha \frac{\text{fluid inertial force}}{\text{gravitational force}} \quad (4.9)$$

$$R_n = \frac{nD^2}{v} = \text{Reynolds number } \alpha \frac{\text{fluid inertial force}}{\text{fluid viscous force}} \quad (4.10)$$

$$M_a = \frac{V}{a} = \text{Mach number} = \frac{\text{mean axial flow velocity}}{\text{speed of sound in the fluid}} \quad (4.11)$$

4.3 Scaling Factors

The scaling factors are defined to represent the parameters that govern the rotor performance by λ denoted as the ratio of model-scale to full-scale parameters. For example, $\lambda_D = D_M/D_F$ is the length scale, which is the ratio of the model-scale diameter (D_M) to the full-scale rotor diameter (D_F). D_M is assumed to be smaller than D_F, and hence $\lambda_D < 1$. When water is used as the fluid medium in a one gravitation (1-g) test facility, $\lambda_g = \lambda_\rho = \lambda_v = \lambda_a = 1$. To preserve the relative motion between the rotor and the inflow, the model-scale and full-scale rotors must operate at the same advance coefficient (*J*). For marine propellers and turbines, it is also important to reproduce the susceptibility to hydrodynamic cavitation. Hence , the model-scale and full-scale rotors must operate at

the same cavitation number (σ_n) in addition to the same *J*, which can be achieved by controlling the pressure inside a cavitation tunnel to match the ambient hydrostatic pressure at the operational depth of the full-scale rotor.

For the same fluid structure-interaction response between the model and the prototype, it is necessary to preserve the same 3D deformation patterns and the same load deformation behavior. The elastic axis and the variation of the center of mass with respect to the elastic axis must be the same between the model and the prototype to achieve the same inertia coupling between bending and torsion. Therefore, the normalized variation of *EI*, *GJ*, and *K* along the radial direction must be the same as the prototype for a geometrically similar model. In addition, the ratio of the elastic bending force to fluid inertial force (α_E), the ratio of the elastic torsional rigidity to bending rigidity (α_{BT}), and the ratio of the elastic bending–twisting coupling rigidity to elastic bending rigidity (α_C) must all be the same between the model and the prototype to achieve the same 3D deformation patterns and load-deformation relationships.

For flexible blades operating in water, the first bending frequency (ω_B) depends on the bending stiffness (K_B), structural mass (M), and hydrodynamic added mass (M_H):

$$\omega_B \alpha \sqrt{\frac{K_B}{M+M_H}}, \quad \text{where} \tag{4.12}$$

$$K_B \alpha \frac{EI}{D^3}, \quad M \alpha \rho_s D^3 \quad and \; M_H \alpha \rho D^3 \tag{4.13}$$

For geometrically similar models, I α D^4, so Eq. (4.12) can be rewritten as follows:

$$\omega_B \alpha \frac{1}{D} \sqrt{\frac{E}{\rho+\rho_s}} \tag{4.14}$$

Similarly, the first torsional frequency can be expressed as follows:

$$\omega_T \, \alpha \, \frac{1}{D}\sqrt{\frac{G}{\rho+\rho_s}} \tag{4.15}$$

The above conditions require six of the nine non-dimensional parameters to be the same between the model and the prototype simulations:

$$\lambda_J = \lambda_{\sigma_n} = \lambda_{\alpha_E} = \lambda_{\alpha_{BT}} = \lambda_{\alpha_C} = \lambda_{\alpha_\rho} = 1 \tag{4.16}$$

Consequently, only three non-dimensional parameters are left: the Froude number (F_n), the Reynolds number (R_n), and the Mach number (M_a). It is well known that the three non-dimensional parameters cannot be satisfied simultaneously unless the model is as large as the prototype, i.e. $\lambda_D=1$. Hence, careful consideration is needed to determine which parameters should be relaxed depending on the objective of the model scale study, and depending on physical limitations of the testing facility and availability/constructability of the rotor material and geometry.

4.4 Relevant Scaling Factors

Since gravitational forces are almost insignificant in the case of marine current turbine, equality in F_n ($\lambda_{Fn}=1$) does not need to be satisfied in order to maintain the same scaling ratio for all four dominant forces in model and full scale. For problems where turbulence or viscous effects are important, it is necessary to satisfy the Reynolds (*Re*) number similarity i.e $\lambda_{Rn}=1$. Equality in *Re* will ensure that viscous forces are correctly scaled. However, such scaling is not easy to achieve in a marine laboratory due to the need to accommodate high relative inflow speed ($\lambda_v=1/\lambda_D$) and high rotor shaft frequency ($\lambda_n=1/\lambda_D^2$). Moreover, it may be difficult to construct a geometrically similar model-scale

rotor that has the same effective structural density, as well as the same normalized bending rigidity, torsional rigidity, and bending–twisting coupling rigidity such that $\lambda_{Ei}= \lambda_{Gij}= 1/\lambda_D^2$ and $\lambda_{vij}= 1$ all along the blade.

Mach number similarity ($\lambda_{Ma}=1$) is important for problems where the influence of flow compressibility is significant. Although, most marine turbines operate in incompressible flow conditions, it may be more practical to conduct laboratory model-scale experiments that satisfy Mach number similarity (i.e. $\lambda_v=1$ if the model and the prototype both operate in the same fluid). Over the years, researchers have demonstrated the validity of theoretical scaling relationships and investigated scaling effects for marine propellers and turbines. The results suggest for most marine rotors where gravitational forces are negligible compared to hydrodynamic inertial force, rotor elastic force, rotor inertial force; it is most practical to conduct model-scale experiments that satisfy Mach number similarity. Moreover, it is cautious although the 3D load- deformation responses will be similar between the Mach-scaled model and the prototype, the detailed stresses and strains distributions, and potential material failure mechanisms, may be different because of differences in production techniques for the model-scale rotor and full-scale rotor.

4.5 Numerical Investigation of Scaling Effects

The validity of the dynamic similarity relationships and scaling effects are demonstrated in the following section.

Table 4.2 gives a summary of the relevant parameters and the relative importance of the Froude number (F_n), the Reynolds number (R_n), and the Mach number (M_a).

Table 4.2: Comparison of scaling factors for a geometrically similar Froude-scaled ($\lambda_{Fn} = 1$), a Reynolds-sacled (($\lambda_{Rn} = 1$)**,** and a Mach-scaled ($\lambda_{Ma} = 1$) composite rotor. Assumptions: $\lambda_g = \lambda_\rho = \lambda_\nu = \lambda_a = 1$ and $\boldsymbol{\lambda_J = \lambda_{\sigma_n} = \lambda_{\alpha_E} = \lambda_{\alpha_{BT}} = \lambda_{\alpha_C} = \lambda_{\alpha_\rho} = 1}$.

Variables	**Symbol**	**Expression**	$\boldsymbol{\lambda_{Fn} = 1}$	$\boldsymbol{\lambda_{Rn} = 1}$	$\boldsymbol{\lambda_{Ma} = 1}$
Froude no.	F_n	$\frac{\lambda_n^2 \lambda_D}{\lambda_g}$	1	$1/\lambda_D^3$	$1/\lambda_D$
Reynolds no.	R_n	$\frac{\lambda_n \lambda_D^2}{\lambda_\nu}$	$\lambda_D^{3/2}$	1	λ_D
Mach no.	M_a	$\frac{\lambda_V}{\lambda_a}$	$\lambda_D^{1/2}$	$1/\lambda_D$	1
Axial velocity	V	λ_V	$\lambda_D^{1/2}$	$1/\lambda_D$	1
Angular velocity	n	λ_n	$1/\lambda_D^{1/2}$	$1/\lambda_D^2$	$1/\lambda_D$
Elastic modulus	E_i	$\lambda_{Ei} = \lambda_n^2 \lambda_D^2$	λ_D	$1/\lambda_D^2$	1
Shear modulus	G_{ij}	$\lambda_{Gij} = \lambda_n^2 \lambda_D^2$	λ_D	$1/\lambda_D^2$	1
Poisson's ratio	ν_{ij}	$\lambda_{\nu_{ij}}$	1	1	1
Elastic force	F_E	$\lambda_E \lambda_D^2$	λ_D^3	1	λ_D^2
Gravitational force	F_G	$\lambda_{\rho s} \lambda_D^3$	λ_D^3	λ_D^3	λ_D^3
Hydrodynamic inertial force	F_H	$\lambda_\rho \lambda_n^2 \lambda_D^4$	λ_D^3	1	λ_D^2
Rotor inertial force	F_I	$\lambda_{\rho s} \lambda_n^2 \lambda_D^4$	λ_D^3	1	λ_D^2
Natural frequencies	ω	$\lambda_\omega = \lambda_n$	$1/\lambda_D^{1/2}$	$1/\lambda_D^3$	$1/\lambda_D$

Table 4.3 shows the models parameters for the full-scale model (λ_D=1) and for 1/2- and 1/8- assumed to satisfy either Froude number (λ_{Fn}=1), Reynolds number (λ_{Rn}) or Mach number (λ_{Ma}) similarities.

Table 4.3: Model parameters used in the numerical simulations. For all the cases, J = 0.9, a = 1500 m/s, g = 9.81 m/s^2, and ν = 0.32

Variable	**Prototype**	**λ_{Fn}=1**		**λ_{Rn}=1**		**λ_{Ma}=1**	
λ_D	**1**	**1/2th**	**1/8th**	**1/2th**	**1/8th**	**1/2th**	**1/8th**
D(m)	20	10	2.5	10	2.5	10	2.5
V (m/s)	2	1.41	0.707	4	16	2	2
n (rpm)	7	9.899	19.799	28	448	14	56
F_n	0.028	0.028	0.028	0.222	14.208	0.055	0.222
R_n (x10^6)	40.9	14.5	1.81	40.9	40.9	20.5	5.12
M_a(x10^{-3})	1.33	0.94	0.47	2.67	10.67	1.33	1.33
E_1 (GPa)	29.7	14.9	37.1	119	1900	29.7	29.7
G_{12}(GPa)	11.3	5.63	1.41	45.0	720	11.3	11.3

Chapter 5

NUMERICAL SIMULATION MODELING, PARAMETRIC STUDIES AND DISCUSSIONS

5.1 Introduction

This Chapter presents the results of numerical simulation and prediction of torque, thrust, and bending moments at the root of rotor blades in a horizontal-axis marine current turbine. Also, the dynamic property of bending moments acting along the blade radius, specifically about the root of the marine current rotors is discussed considering the variation of wave height, rotor rotational speed and current speed (Senat and Arockiasamy, 2011). The measured current velocities near the core of Florida current offshore are used in the evaluation of the loads on the full-scale rotor blades (Fig. 5.1). Figs. 5.2 and 5.3 show the experimental South Florida Gulfstream and Wave Forecasts using the Simulating Waves Nearshore (SWAN) wave model and the Real Time Ocean Forecast System.

Since the available power generation levels are directly related to the marine current velocity, it is essential to describe statistically the marine current velocity distributions. The description of the current characteristics will yield the energy content

of the currents on a given site and their energy distribution. The energy content determines whether it is worthwhile installing a turbine on any given site and the energy distribution provides us with information about the prevalent current speeds to help with the turbine design. In the present study numerical simulations are carried out using a mathematical model to generate the hydrodynamic forces and bending moments on the 20 m diameter tri-bladed horizontal-axis turbine.

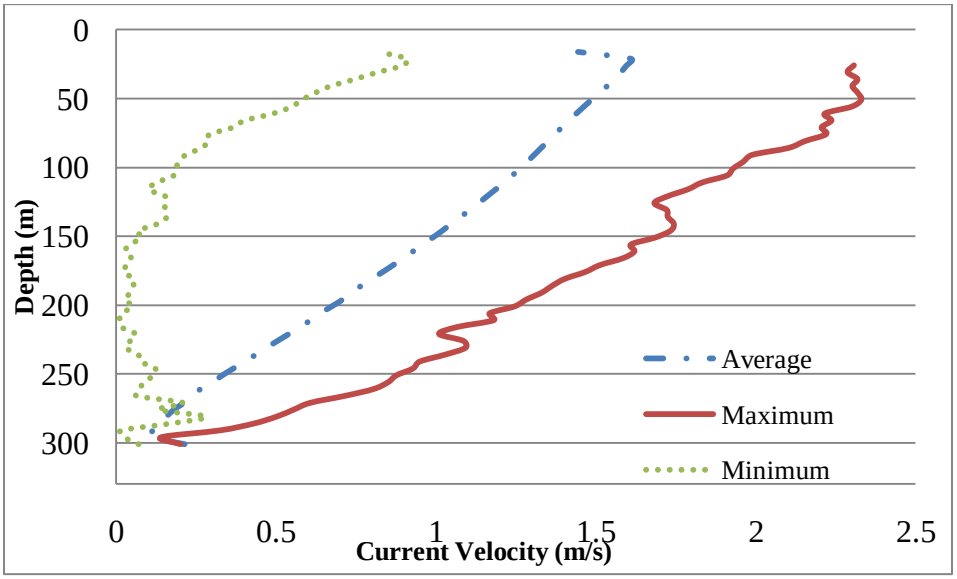

Figure 5.1: The maximum, average, and minimum ocean current speed measured offshore ft. lauderdale, fl over a period of nearly 2 years. velocity measurements were made at 15 minute intervals with a 75 kHz ADCP.

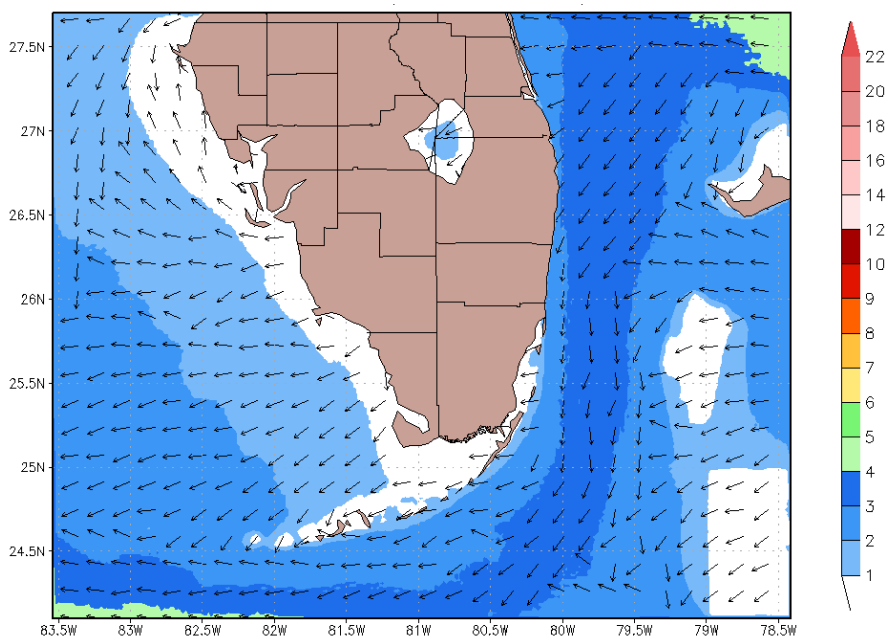

Figure 5.2: Significant Wave Height (ft) and Peak Wave Direction for South Florida (source: NOAA, WFO MIA SWAN forecast)

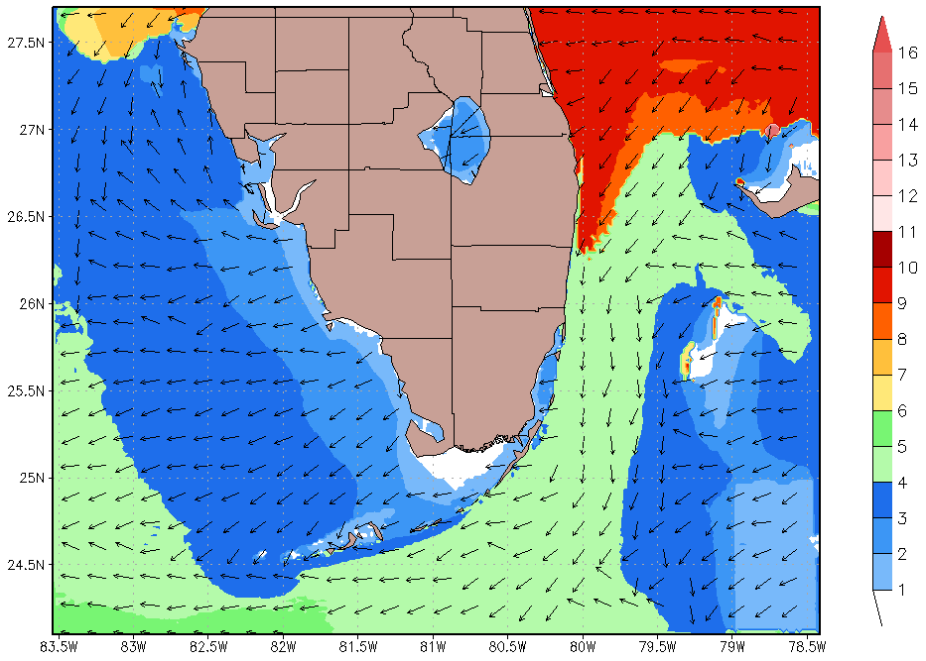

Figure 5.3: Peak Wave Period (s) and Direction for South Florida (Source: NOAA, WFO MIA SWAN forecast)

The model rotor has essentially a wind turbine configuration with a slight increase in blade chord and thickness for structural strength. The rotor uses three blades and has a diameter of 20 m. The blades merge into the hub without taper and its angles can be adjusted over a range of limited degrees. The blade section used in the study follows the section S814 developed by Somers (1992). The S814 is one of the series created by the NREL, USA for wind turbines. One important characteristic of the S814 is the minimal sensitivity of its maximum lift coefficient to roughness effects, which is a critical property for stall-regulated wind turbines. The aerofoil has a very low drag coefficient and is also not too sensitive to change of angle of attack around the stalling angle. In general, the aerofoil profile for the blade is chosen based on its good performance at low Reynolds number and its tolerance to surface imperfections (Barltrop et al., 2007)..

In the simulation model, numerical calculations are carried out for every time step on the assumption of quasi-steady flow. The rotor parameters are defined based on the pitch angle, coning angle, hub radius, and root radius. Interpolation functions are defined for twist angle and chord length along the blade length. The torque, thrust and bending moments induced by the stream flow are calculated using MathCAD. Lift and drag coefficients are determined as function of incident angles taking into account the 3D effects. Limited parametric studies are carried out to better understand the influence of important parameters on the performance of the rotor. Simulated thrust and torque are obtained when rotor operates in calm water and waves. The variation in the thrust and torque is predicted for certain parameters including wave height and wave frequency. The thrust and torque are evaluated by varying both the rotor's rotational speed and current speed.

5.1.1 Characteristic Variation of the Force Coefficients.

Figure 5.4 presents the characteristic variation of lift and drag coefficients with the azimuthal angle between -180 and 180 degrees. In the simulation, the three-dimensional effects on the lift coefficients are considered and the lift coefficients computed based on two-dimensional lift coefficients using the following equation.

$$C_{L-3D} = C_{L-2D} + \Delta C_L \times 3\left(\frac{c(r)}{r}\right)^2 \qquad (5.1)$$

where ΔC_L is the difference between C_L obtained from linear potential flow theory and the actual two-dimensional lift coefficient C_{L-2D} . $c(r)$ is the chord length which is a function of radial distance r from the root. This equation has the effect of extanding the attack angles before stall occurs. The drag coefficient is assumed to be equal to the two-dimensional drag coefficient. Coefficients were specified for a range of attack angles and intermediate coefficients estimated using linear interpolation (Barltrop et al., 2006).

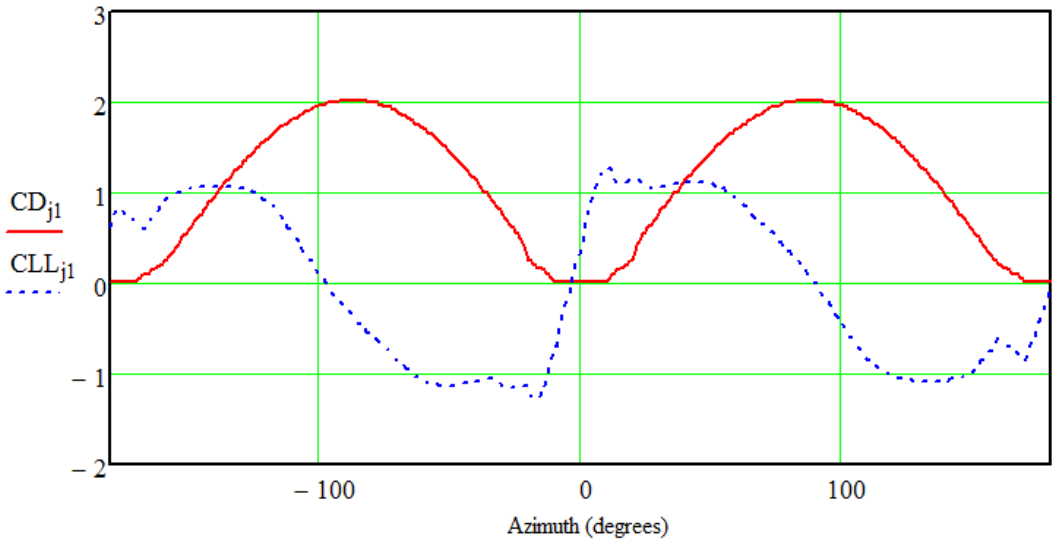

Figure 5.4: Variation of lift and drag coefficients with the azimuthal angle between -180 and 180 degrees.

5.1.2 Dynamic Response Properties of the Rotor with Variation of Wave Height, Rotor Rotational Speed, and Current Speed.

Simulations were carried out to examine the performance of the marine current turbine rotor for different conditions. The most important parameters were the dynamic properties of the rotor under different wave heights, wave frequencies, and current speeds. The investigation covered a range of simulated current speeds (2.0, 2.5 and 3.0 m/s), wave heights (3.0 and 5.0 m), and rotor rotational speeds (7, 10 and 14 rpm). The parametric studies were focused to examine the variations of thrust, torque, and bending moments induced in the full-scale rotor.

The full-scale mathematical model rotor was simulated for a condition where the wave-current interactions are considered for analysis of the hydrodynamic loading effects on the blades. The results show the variation of the steady state torque, thrust, moments experienced by the turbine in time domain. The torque acting on the rotor is calculated as the sum of torque acting on individual blade, which is basically the sum of products of in-plane lift and drag forces and the arm lengths from center of blade elements to the axis of the rotor. Similarly, thrust on the rotor is equal to the sum of out-of-plane lift and drag forces on blade sections of all blades on the rotor. Figure 5.5a shows the mean torque in the rotor blades due to the wave heights of 3.0 m and 5.0 m, wave period of 10 s, current speed of 2.0 m/s and rotational speed of 7 rpm. It can be observed from Figure 5.7 that the magnitude of mean torque increase is twice with increases in the wave height to 5.0 m, rotational speed to 14 rpm, and current speed to 3.0 m/s. Earlier researchers have

reported that the presence of waves tends to increase the torque at lower range of current speed (up to 0.8 m/s) in a model-scale rotor (Somers, 1997).

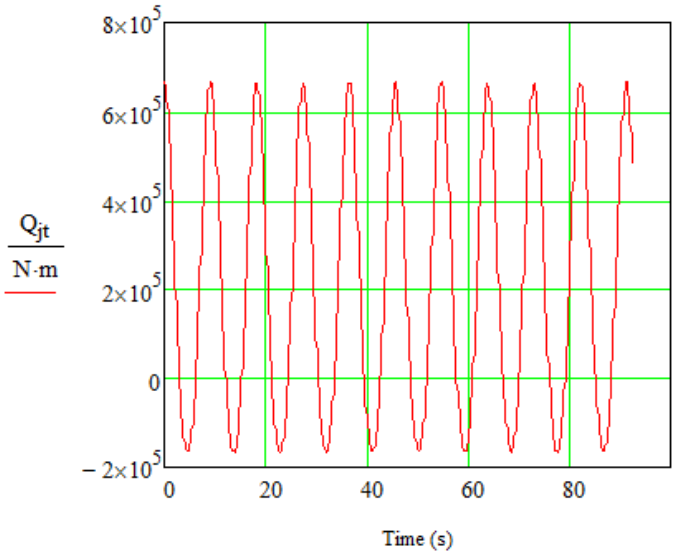

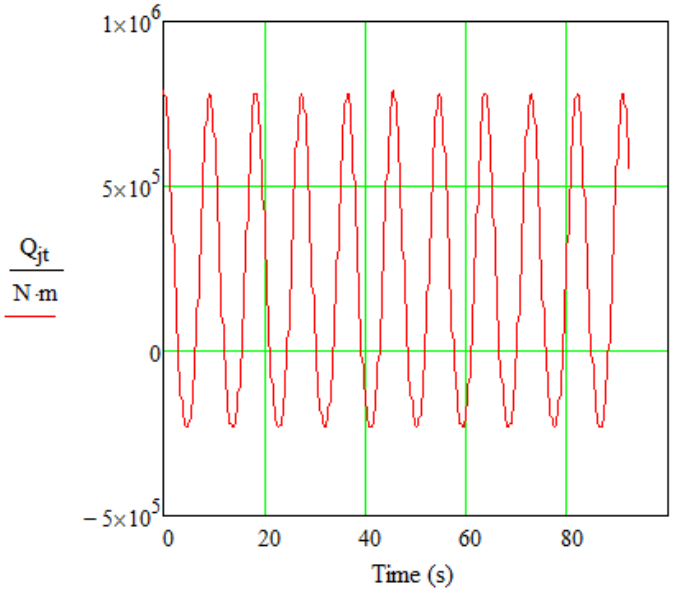

Figure 5.5:(a) Time history of torque, Q_{jt} , in waves of 3.0 m height wave period of 10 sec., rotational speed of 7 rpm and current speed of 2.0 m/s at full-scale model.

(b) Time history of torque, Q_{jt} , in waves of 5.0 m height , wave period of 10 sec, rotational speed of 7 rpm and current speed of 2.0 m/s at full-scale model.

Figure 5.5(b) shows that in wave of 0.733 Hz, when wave height increases from 3.0 m to 5.0 m, the range of variation of torque on the rotor is significantly increased. On the other hand, Figure 5.6a shows the time history of torque in the rotor blades in waves of 3.0 and 5.0 m height, wave period of 5 s, rotational speed of 7 rpm and current speed of 2.0 m/s. The torque values increase about 64% for the same rotational speed of 7 rpm, current speed of 2.0 m/s and increased in wave height to 5.0 m (Fig.5.6b).

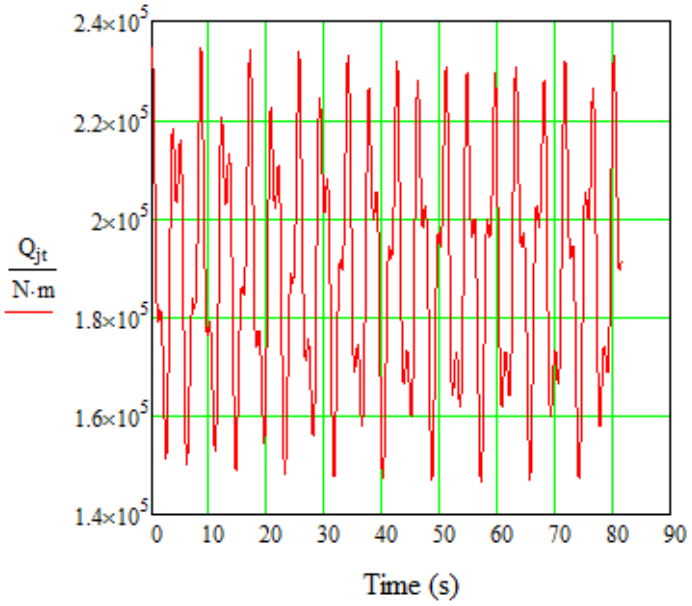

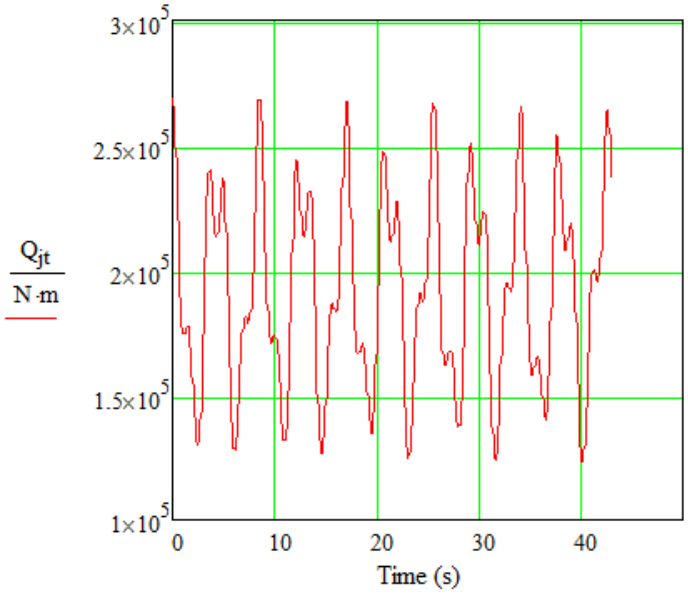

Figure 5.6: (a) Time history of torque, Q_{jt} , in waves of 5.0 m height , wave period of 5 sec, rotational speed of 7 rpm and current speed of 2.0 m/s at full-scale model.

(b) Time history of torque, Q_{jt} , in waves of 5.0 m height , wave period of 5 sec, rotational speed of 7 rpm and current speed of 2.0 m/s at full-scale model.

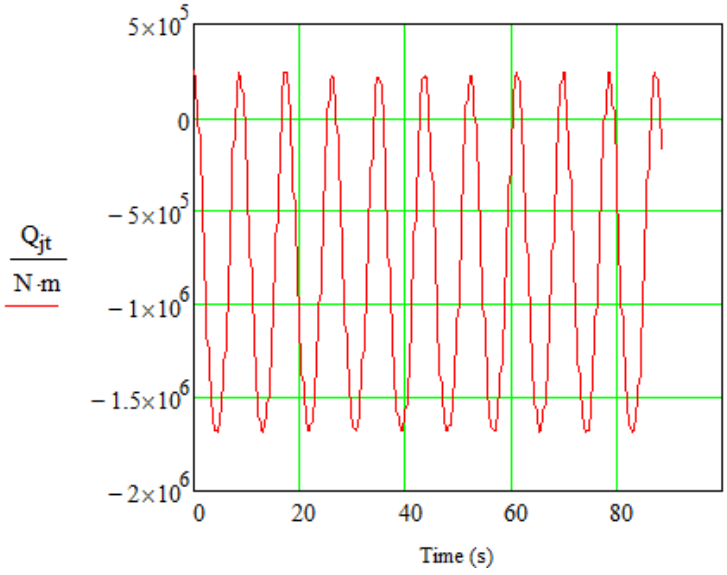

Figure 5.7: Time history of torque, Q_{jt} , in waves of 5.0 m height , rotational speed of 14 rpm, and current speed of 3.0 m/s at full-scale model

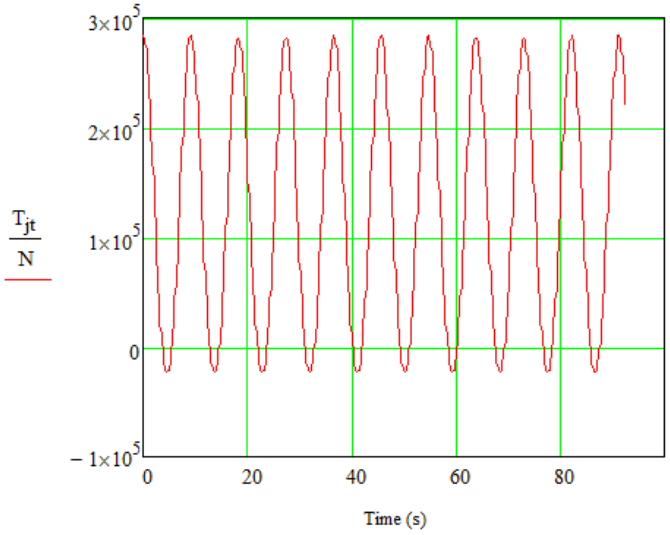

Figure 5.8: Time history of thrust, Tjt, in waves of 3.0 m height, rotational speed of 7 rpm, and current speed of 2.0 m/s at full-scale model.

Figure 5.8 shows the time history of thrust in the rotor blades in waves of 3.0 m height, rotational speed of 7 rpm, and current speed of 2.0 m/s. The thrust values increase about 33% for the same wave height, increased rotational speed of 10 rpm, and increased current speed of 2.5 m/s (Fig.5.9).

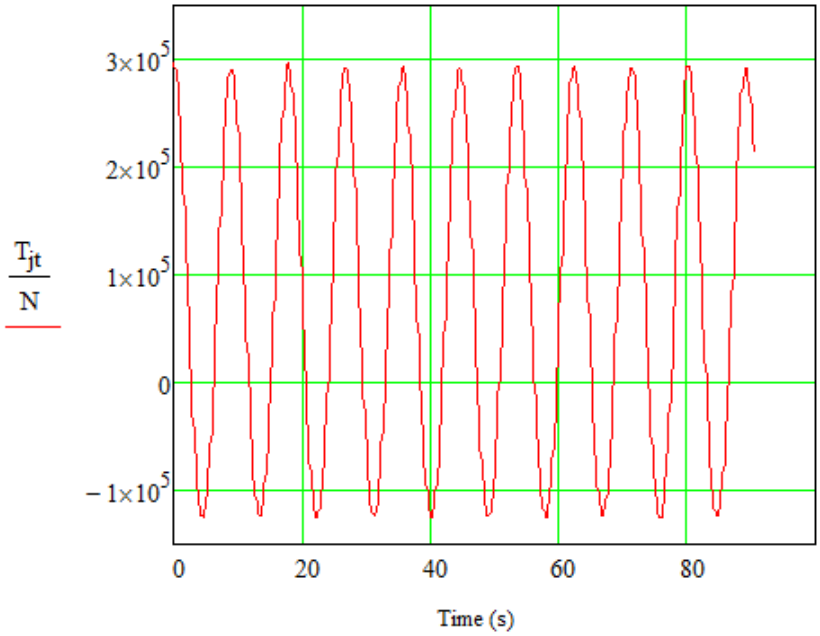

Figure 5.9: Time history of thrust, Tjt, in waves of 3.0 m height, rotational speed of 10 rpm, and current speed of 2.5 m/s at full-scale model.

Bending moments acting around the root of each blade are calculated in the same manner as the thrust and torque forces. The out-of-plane moment is determined as the sum of products of out-of-plane lift and drag forces and the arm lengths from the center of the blade sections to the root of the blade. On the other hand, the in-plane moment is calculated as the sum of products of in-plane lift and drag forces and the arm lengths from centers of blade sections to the root of the blade.

The in-plane bending moment range at the root of the rotor blade is approximately 25% of the out-of-plane bending moment (Figs.5.10 and 5.11). Figure 5.9 shows the out-of-plane and in-plane bending moments in waves of 3.0 m height, current speed of 2.0 m/s, and rotational speed of 7 rpm. The maximum out-of-plane bending moment range is 0.8×10^6 N-m. The maximum out-of-plane bending moment range increases by more than 100% for the case with waves of 5.0 m height, current speed of 3.0 m/s, and rotational speed of 14 rpm (Fig. 5.11).

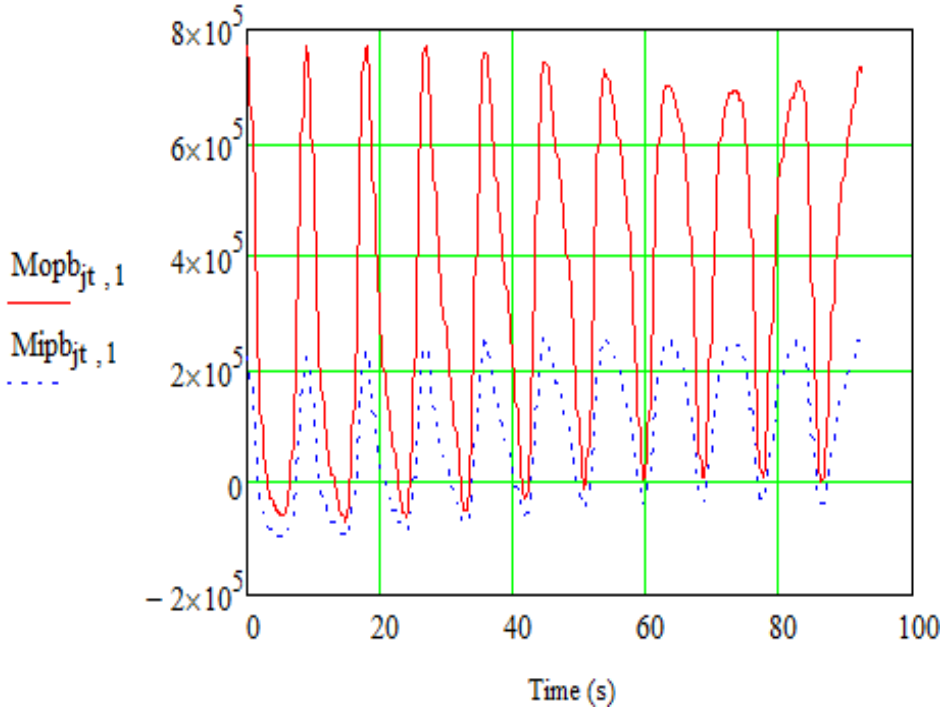

Figure 5.10: Out-of-plane and in-plane bending moments, $Mopb_{jt}$, and $Mipb_{jt}$, respectively, in waves of 3.0 m height, rotational speed of 7 rpm and current speed of 2.0 m/s at full-scale model.

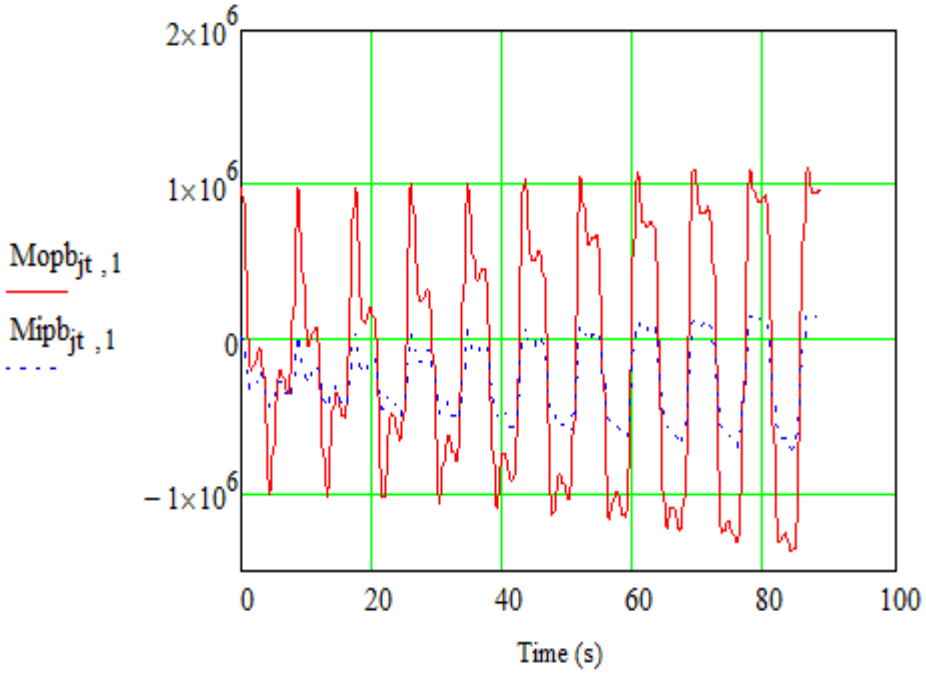

Figure 5.11: Out-of-plane and in-plane bending moments, $Mopb_{jt}$, and $Mipb_{jt}$, respectively, in waves of 5.0 m height, rotational speed of 14 rpm and current speed of 3.0 m/s at full-scale model.

For a pitch angle of 4.22 degrees, the mean torque acting on the rotor is 0.1442 MN-m and the mean power generated corresponding to a hypothetical full scale rotor of 20 m diameter rotating at 7 rpm in waves of 3.0 m height and 10 s period along with a current speed of 2.0 m/s is 0.1057 MW.

5.2 Parametric Studies

Figures 5.12 and 5.14 show the effect of waves and the variations of wave frequency on thrust and torque at a rotational speed of 7 rpm. The presence of waves does not appear to make any significant changes to both the mean torque and thrust. This may be attributed to the small difference between the two frequencies considered in the study.

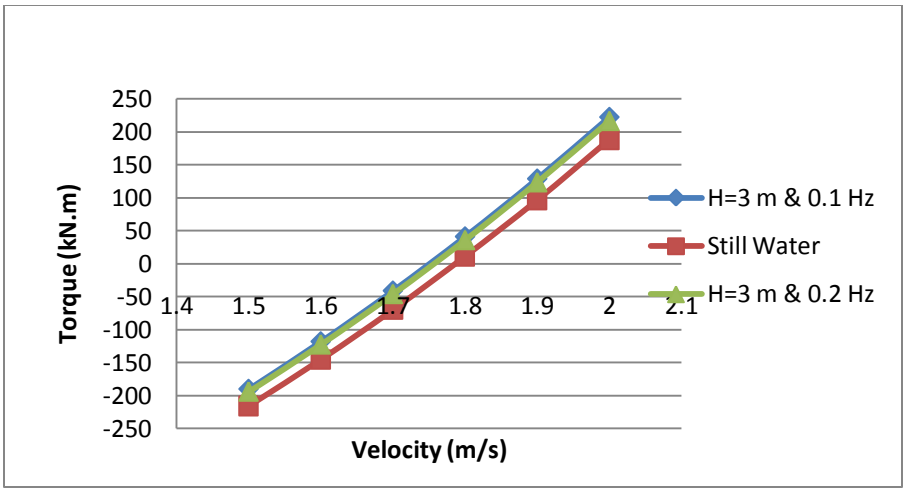

Figure 5.12: Effects of wave frequency on mean torque and thrust when rotor rotates at 7 rpm.

Figure 5.13 and 5.15 show both torque and thrust generally increase with increased current speed. A steady trend in the increase in the mean torque can be seen from Figure 5.12 with increase in the height of incident waves. However, the mean thrust appears to be relatively unchanged (Fig. 5.15).

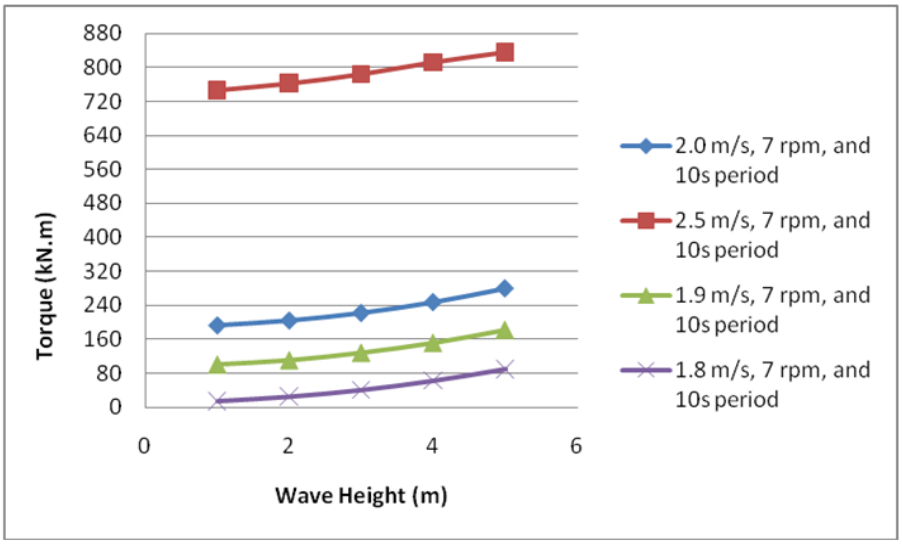

Figure 5.13: Effects of wave height on mean torque when rotor rotates at 7 rpm in waves of 0.10 Hz

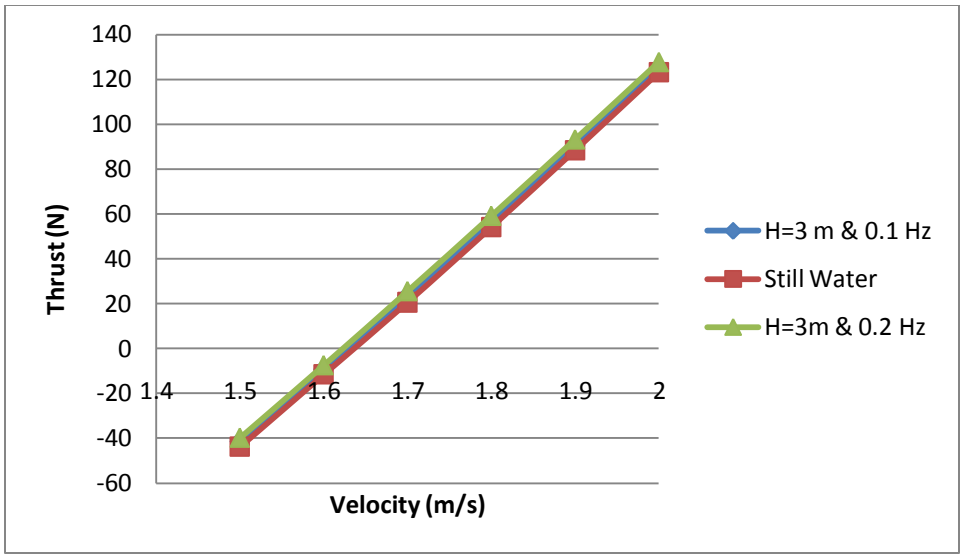

Figure 5.14: Effects of wave frequency on mean thrust when rotor rotates at 7 rpm

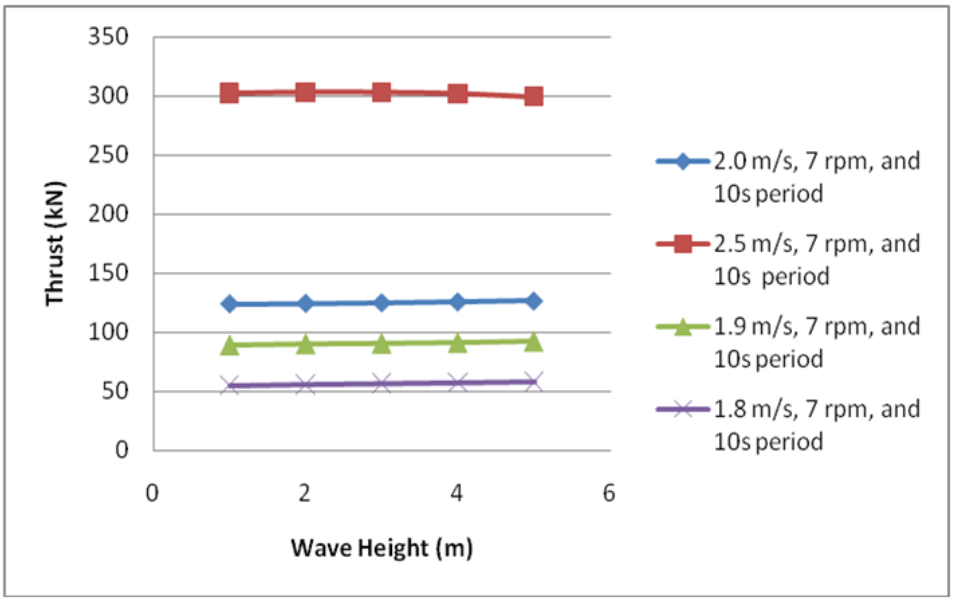

Figure 5.15: Effects of wave height on mean thrust when rotor rotates at 7 rpm in waves of 0.10 Hz.

5.3 Performance Characteristics of the Model Turbine

The performance of a 20 m diameter rotor operating in marine currents with a velocity of 2.5 m/s is evaluated using BEM theory. The power and thrust coefficients (Cp and CT) are computed for a set hub pitch angles 0^o, 5^o, and 12^o. The results show a reduction of C_p and C_T as hub pitch angle is increased, with a maximum of C_P=0.49 for the design 5^o pitch angle. The coefficient C_p and C_T show very little variations for the tip speed ratios (TSR) in the range of 4-5 (Fig. 5.17). The thrust coefficient (C_T) reduces significantly as the pitch angle increases from 0^o to 12^o (see Fig. 5.18). However, the power coefficient C_p does exhibit only small changes in the magnitude. BEM theory can be effectively used to predict the power and thrust coefficients for the rotor for the case of marine currents.

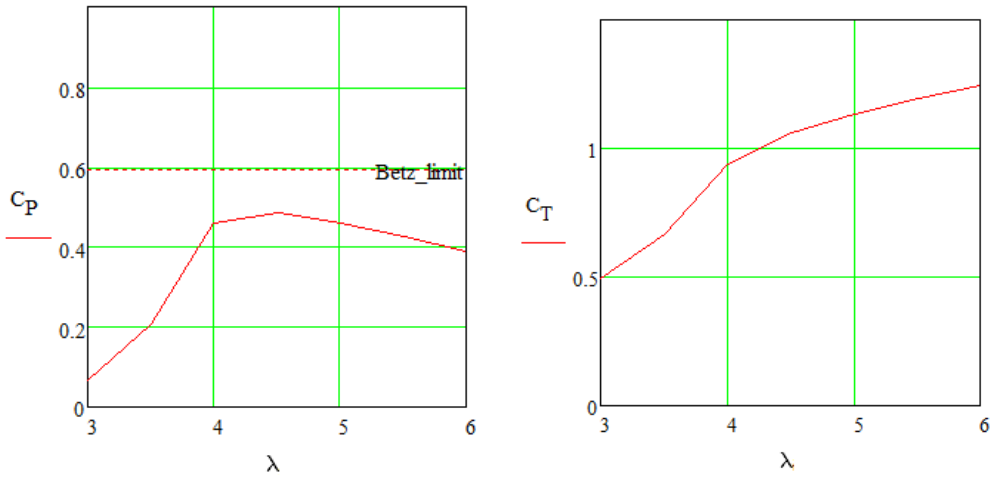

Figure 5.16: Simulations Cp and C_T with a 0^o set pitch angle

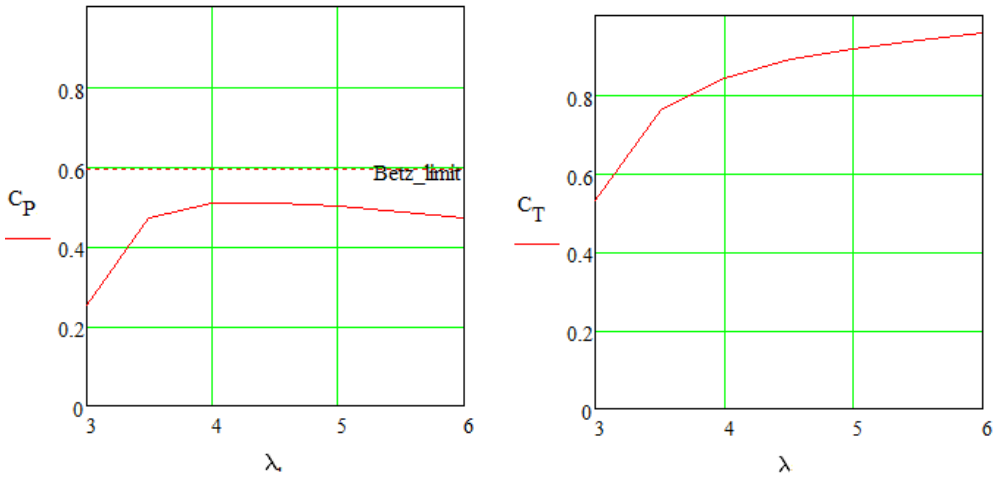

Figure 5.17: Simulations Cp and C_T with a 5^o set pitch angle

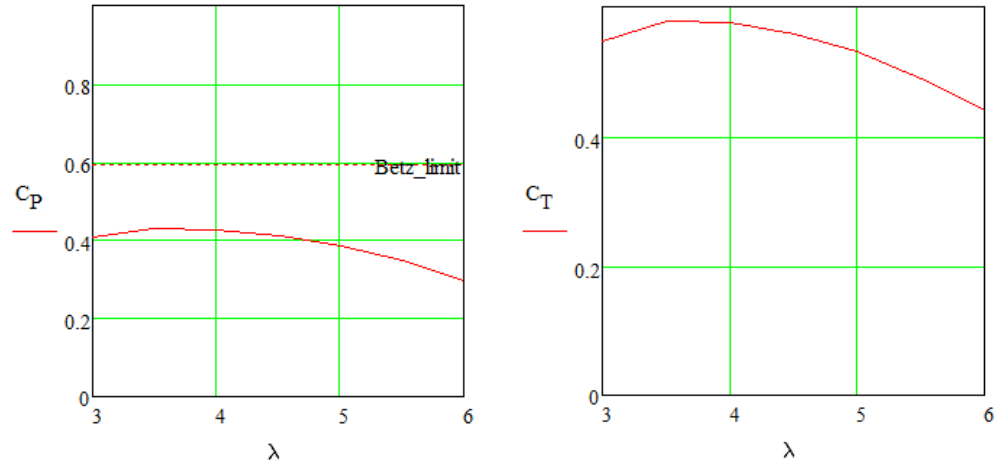

Figure 5.17: Simulations Cp and C_T with a 12^o set pitch angle

Table 5.1: Power and thrust values simulated with a set of pitch angles (0^o, 5^o, 12^o) for a 20 m diameter turbine in a 2.5 m/s marine current.

		Power (MW)			Thrust (kN)		
Tip speed ratio,λ		4	5	6	4	5	6
Pitch angle	0^o	0.0135	0.012	0.01	47	56	61
	5^o	0.0147	0.0014	0.013	41	46	47
	12^o	0.012	0.011	0.008	28	26	22

Table 5.2: Power and thrust values simulated with a set of pitch angles (0^o, 5^o, 12^o) for a 20 m diameter turbine in a 2.5 m/s combined marine current and wave.

		Power (MW)			Thrust (kN)		
Tip speed ratio,λ		4	5	6	4	5	6
Pitch angle	0^o	0.318	0.313	0.318	229	225	243
	5^o	0.706	0.704	0.706	397	396	397
	12^o	0.501	0.395	0.503	269	212	263

The power and thrust values for a 20 m rotor operating in marine currents with a velocity of 2.5 m/s are presented in Table 5.1. As the pitch angle increases, the values show very little variations for the design cases, especially for set angle 5^o and TSR in the range of 4-6. However, the trend is reversed for the thrust values when the pitch angle is set above 10^o. On the other hand, Table 5.2 presents mean power and thrust values simulated with a set of pitch angles (0^o, 5^o, 12^o) for the same rotor in a 2.5 m/s marine currents with wave of 3.0 m height and 10 s period. The values show very little variations for the design case of 5^o pitch angle and TSR in the range of 4-6. However, both the mean power and thrust values increase when considering the combined effect of marine current and waves.

Chapter 6

SUMMARY, CONCLUSIONS AND FUTURE WORK

6.1 Summary

- The measured current velocities near the core of Florida current offshore are used in the evaluation of the loads on the full-scale rotor blades in a horizontal axis marine current turbine.
- In the simulation model, numerical calculations are carried out on the assumption of quasi-steady flow and the torque, thrust and bending moments induced by the stream flow are calculated using MathCAD.
- Lift and drag coefficients are determined as function of incident angle taking into account the 3D effects.
- Simulated thrust and torque are obtained in calm water and waves including parameters-wave height, wave frequency, rotor rotational speed and marine current speed.
- The power and thrust coefficients are computed for a set of hub pitch angles and tip speed ratios.
- A summary of the scaling factors for the various fluid and structural parameters that control the dynamic interaction between the flexible marine rotor and the

- surrounding flow is presented along with the model parameter for the full-scale model (λ_D=1) and for 1/2-and 1/8- scaled models assumed to satisfy either Froude number (λ_{Fn}=1), Reynolds number (λ_{Rn}=1) or Mach number (λ_{Ma}=1) similarities.

6.2 Conclusions

- The blade element-momentum theory combined with linear wave theory can be used to analyze the wave-current interactions in marine current turbine.
- In steep waves, the out-of-plane bending moment fluctuates significantly by more than 100% for the case with waves of 5.0 m, current speed of 3.0 m/s and rotational speed of 14 rpm compared to waves of 3.0 m, current speed of 2.0 m/s and rotational speed of 7 rpm.
- In longer waves (T_w=10 sec against T_w=5 sec), the increase in wave height contributes a greater effect on the rotor torque.
- For a given current speed, the torque on the rotor increases with increase in wave heights whereas the axial thrust remains unchanged.
- Waves approaching along the normal to the rotor plane lead to the largest bending moment on the blades.
- For most marine rotors where gravitational forces are negligible compared to hydrodynamic inertial force, rotor elastic force, rotor inertial force, it is most practical to conduct model scale experiment that satisfy Mach number similarity, i.e. λ_v=1.
- The power coefficient C_p and the thrust coefficient C_T show very little variations for the tip speed ratios (TSR) in the range of 4-5. The thrust

coefficient (C_T) reduces significantly as the pitch angle increases from 0^o to 12^o, whereas the power coefficient C_p does exhibit only small changes in the magnitude.

6.3 Future Work

- The characterization of the turbulence effects on the behavior of the turbine rotor needs to be done to evaluate the impact that the high loading fluctuations on the blade could have on the fatigue of the structure.
- The blade deformation requires further study in order to quantify flow effects on the fatigue of the structure.
- Further study on the wake effect due to the proximity between the turbine rotor and the sea bed shall provide data on the added turbulence.

REFERENCES

Baltazar, J., & Falcao de Campos, J.A.C. (2009). Unsteady analysis of a horizontal axis marine current turbine in yawed inflow conditions with a panel method. Proceedings of the First International Symposium on Marine Propulsors. Trondheim, Norway:

Barltrop, N, K.S. Varyani, A Grant, D Clelland, and Xuan Pham. "Wave-current interactions in marine current turbines." Engineering for the Maritime Environment. 220.M (2006).

Barltrop, N, K.S. Varyani, A Grant, D Clelland, and Xuan Pham. "Investigation into wave-current interactions in marine current turbines." Proc. IMechE Vol. 221 Part A: J. Power and Energy (2007), pp.233-242.

Batten, W.M.J., Bahaj, A.S., Molland, A.F., & Chaplin, J.R. (2006). Hydrodynamics of marine current turbines. Renewable energy, 31, 249-256.

Batten W.M.J, Bahaj A.S., Molland AF, Chaplin JR. Experimentally validated numerical method for the hydrodynamic design of horizontal axis tidal turbines. Ocean Engineering (2007);34(7):1013–29.

Batten W.M.J, Bahaj A.S., Molland AF, Chaplin JR. Yawed performance of horizontal axis turbines in marine currents, In: Proceedings of the second international conference of renewable energy in Maritime Island Climates—Dublin, 2006, p. 39–46.

Boud, R. (2003). Status and Research and Development Priorities, Wave and Marine Current Energy. UK: International Energy Agency. Web. 11 Apr 2010.

Burton, T.; Sharpe, D.; Jenkins, N.; Bossanyi, E. (2001). Wind Energy Handbook. Wiley.

Charlier, R.H. (2007). Forty candles for the Rance River TPP tides provide renewable and sustainable power generation, Renewable and Sustainable Energy Reviews, 11, 2032-2057.

Driscoll, F.R., Alsenas, G.M., Beaujean, P.P., Ravenna, Shirley, Raveling, Jason, Busold, Erick, and Slezycki, Caitlin. "A 20KW Open Current Test Turbine." Center for Ocean Energy Technology. (2006).

Eggleston, D.M. and Stoddard, F.S.Wind turbine engineering design, 1978 (Van Nostrand Reinhold, New York).

Fraenkel, P.L. (2002). Power from marine currents. *Proc Instn Mech Engrs Vol 216 Part A:* J Power and Energy (pp. 1-14).

The Carbon Trust, Future Marine Energy, January 2006.

Germanicher Lloyd (GL) WindEnergie (2005). "Guideline for the Certification of Ocean Energy Converters, Part1: Ocean Current Turbines".

DNV Draft (2004). Guideline on the assessment and application of Standards and Recommended Practices for Wave Energy Conversion Devices.

ISSC Committee V.4: Ocean, Wind and Wave Energy Utilization.

Lemanski, L. F., Coley, C.E., Goldberger, G. N., Dhanak, M. R., and Driscoll, F. R. (2008) "Center of Excellence in Ocean Energy Technology, Technical Proposal: pp.1-18. <http://www.fau.edu/bot/files/COEOET_Doc.pdf>

Maganga,F.,Germain, G., King, J., Pinon, G., Rivoalen, E.. "Experimental study to determine flow characteristic effects on marine current turbine behavior". Proceedings of the 8th European Wave and Tidal Energy Conference, Uppsala, Sweden, (2009).pp.661-667.

Marine Current Turbines Ltd., http://www.marineturbines.com.

McCormick, M.E. (2010). Ocean engineering mechanics. New York: Cambridge University Press

Mineral Management Services, (2006). Ocean current energy potential on the U.S. outer continental shelf. Washington, DC: U.S. Department of the Interior.

Molland, A.F., A.S. Bahaj, J.R. Chaplin, and W.M.J Batten. "Measurements and predictions of forces, pressures and cavitation on 2-D sections suitable for marine current turbines." Engineering for the Maritime Environment. 218.M (2004): Print.

Molland, A.F., A.S. Bahaj, J.R. Chaplin, and W.M.J Batten. "Hydrodynamics of marine current turbines." Engineering for the Maritime Environment (2005).

Myers, L.E., & Bahaj, A.S. (2009). Experimental analysis of the flow field around horizontal axis tidal turbines by the use of scale mesh disk rotor simulators. Ocean Engineering, 37, 218-227.

European Marine Energy Center (EMEC) Limited (2004). "Performance assessment for wave energy conversion systems in open sea test facilities".

Senat, J., and Arockiasamy, M. "Simulation and Prediction of Loads in Marine Current Turbine Full-Scale Rotor Blades." Proceedings of the ASME 2011 30th International Conference on Ocean,Offshore and Arctic Engineering. Rotterdam, ASME. 2011. Print.

Somers, D. M. The airfoil S814 and S815 airfoil, 1992 (Airfoil Inc.).

Somers, D. M. Design and experimental results for the S814 airfoil. NREL/SR-440-6918, UC Category:1213, DE97000104, 1997.

Young, Y.L. (2010). Dynamic hydroelastic scaling of self-adaptive composite marine rotors. Composite Structures, 92, 97-106.

U.S. Census Bureau, "Interim Projections of the Total Population for the United States: April 1, 2000 to July 1, 2030," 2005. http://www.census.gov

Wang, S., Lu, L., Li, D., Shan, Z., & Zhao, L. (2008). Experimental study on flexible blade turbine driven by tidal current energy. Chinese-german joint symposium on hydraulic and ocean engineering, pp.333-338.

W.E. de Vries, J. van der Tempel, H. Carstens, K. Argyriadis, P. Passon, T. Camp, R.Cutts. Assessment of bottom-mounted support structure types with conventional design stiffness and installation techniques for typical deep water sites, Deliverable D4.2.1 (WP4: Offshore foundations and support structures), Project UpWind EU Contract No.: 019945 (SES6) "Integrated Wind Turbine Design", http://www.upwind.eu.